

AQ: #1 **1 Error distribution in randomly perturbed orbits**

2 Ph. Marie,^{1,a)} G. Turchetti,^{2,b)} S. Vaienti,^{1,3,c)} and F. Zanlungo^{2,d)}
 3 ¹Centre de Physique Théorique, CNRS, UMR-6207, Universités d'Aix-Marseille I, II,
 4 Provence-Alpes-Côte-d'Azur 13284, France and Université du Sud, Toulon-Var, Toulon 83130, France
 5 ²Department of Physics and Centro Galvani, University of Bologna, Bologna 40126, Italy
 6 ³Fédération de Recherche des Unités de Mathématiques de Marseille (FRUMAM), CPT,
 7 Luminy Case 907, F-13288 Marseille Cedex 9, France

8 (Received 18 May 2009; accepted 3 November 2009; published online xx xx xxxx)

9 Given an observable f defined on the phase space of some dynamical system generated by the map
 10 T , we consider the error between the value of the function $f(T^n x_0)$ computed at time n along the
 11 orbit with initial condition x_0 , and the value $f(T_\omega^n x_0)$ of the same observable computed by replacing
 12 the map T^n with the composition of maps $T_{\omega_n} \circ \dots \circ T_{\omega_1}$, where each T_ω is chosen randomly, by
 13 varying ω , in a neighborhood of size ε of T . We show that the random variable $\Delta_n^\varepsilon \equiv f(T^n x_0)$
 14 $- f(T_\omega^n x_0)$, depending on the initial condition x_0 and on the choice of the realization ω , will converge
 15 in distribution when $n \rightarrow \infty$ to what we call the *asymptotic error*. We study in detail the
 16 density of the distribution function of the asymptotic error for a wide class of dynamical systems
 17 perturbed with additive noise: for a few of them we give rigorous results, for the others we provide
 18 a numerical investigation. Our study is intended as a model for the effects of numerical noise due
 19 to roundoff on dynamical systems. © 2009 American Institute of Physics. [doi:10.1063/1.3267510]
 20

21 **In the present paper we study the effect of a random**
 22 **perturbation on the orbit of a discrete dynamical system.**
 23 **We analyze the statistics of global errors Δ_n^ε , i.e., of the**
 24 **algebraic difference at iteration n between the exact orbit**
 25 **and an orbit perturbed at each step with a random error**
 26 **of order ε , by providing exact results for two model**
 27 **maps, regular and chaotic, respectively, and stating a**
 28 **general theorem on their asymptotics. This analysis sug-**
 29 **gests the existence of a time scale depending on ε for the**
 30 **convergence to the asymptotic error distribution. The**
 31 **scale is basically $\log(1/\varepsilon)$ for chaotic maps and ε^{-2} for**
 32 **regular maps and it is related to the interplay of the noise**
 33 **with the exponential or linear divergence of nearby or-**
 34 **bits. The present paper provides, on rigorous grounds,**
 35 **the framework suitable to perform a systematic analysis**
 36 **of the statistics of the global error due to roundoff. In a**
 37 **future work and by using the numerical tools developed**
 38 **here, we will compare the results of this paper with those**
 39 **obtained using pure roundoff noise to check if the same**
 40 **qualitative behavior (i.e., the same time scales for the**
 41 **convergence to the asymptotic error distribution) holds.**
 42

43 I. INTRODUCTION

44 The reliability of numerical computations for discrete
 45 dynamical systems, where the only source of errors is due to
 46 the representation of real numbers by finite strings and to
 47 roundoff in arithmetic operations, is a long standing ques-
 48 tion. The algorithms used to implement roundoff arithmetic
 49 are not universal but depend on the hardware. As a conse-

quence a rigorous analysis of the propagation of errors due to
 roundoff in floating point computations is largely
 incomplete.¹ The relative error η defined by $x^* = x(1 + \eta)$,
 where x^* is the floating point representation of the real number
 x , grows when an iterative procedure is applied and the
 numerical orbit $x_n^* = T_* x_{n-1}^*$ may diverge with respect to the
 true orbit $x_n = T x_{n-1}$, where T is the map acting on the space
 X and T_* is its floating point representation. We also stress
 that the numerical inverse of a map T_*^{-1} , computed by imple-
 menting the algorithm which defines the true inverse T^{-1} , is
 not exact. The distance $d(\cdot, \cdot)$ between the true orbit and the
 numerical one is in general not known; however if in a single
 iteration it remains bounded $d(x_{n+1}^*, T x_n^*) \equiv d(T_* x_n^*, T x_n^*) < \varepsilon$,
 then we say that the numerical orbit is an ε pseudo-orbit, and
 some theoretical results are available if the map is mixing.

The reversibility error after n iterations $d(x_*, T_*^{-n} \circ T_* x_*)$
 has a growth rate comparable to $d(T^n x_*, T_*^n x_*)$. Even though
 arithmetic with roundoff is deterministic it is often assumed
 that the sequence of errors is random. If so, letting $T x_n^* -$
 $T_* x_n^* = \varepsilon \xi_n$, the pseudo-orbit x_n^* appears to be generated by a
 map $T_* x = T x + \varepsilon \xi$ randomly perturbed with an additive noise.
 To prove that for any given initial point x_* the sequence ξ_n is
 actually equivalent to the realization of a random process and
 to specify its properties is once more a hard theoretical task.
 Nevertheless it is possible to investigate numerically the sta-
 tistics of the pseudorandom sequence ξ_n by evaluating T with
 a much higher accuracy with respect to T_* so that we may
 neglect the difference with the exact result, at least below a
 significant time scale. To carry out this program it is critical
 to have some analytical estimates to guide our numerical
 investigations. In particular we need to know how the statis-
 tics of global errors $\Delta_n = T_*^n x_* - T^n x$ changes, evolving from
 the initial distribution $\rho_0(x) = \delta(x)$ to the asymptotic distribu-
 tion $\rho_\infty(x)$. This program differs radically from the search of

^{a)}Electronic mail: pmarie@cpt.univ-mrs.fr.

^{b)}Electronic mail: turchetti@bo.infn.it.

^{c)}Electronic mail: vaienti@cpt.univ-mrs.fr.

^{d)}Electronic mail: zanlungo@bo.infn.it.

84 a true orbit, close to the pseudo-orbit, whose existence is
85 assured by the shadowing lemma.²⁻⁸

86 In the present work we compare the true orbit $T^n x_0$ and
87 an ε -pseudo-orbit $\{x'_n\}_{n \geq 0}$ starting from the same initial point
88 x_0 and analyze the probability distribution function of the
89 algebraic error $f(T^n x_0) - f(x'_n)$, where f is a smooth observ-
90 able over X . More specifically we consider the case in which
91 the pseudo-orbit is a random perturbation of the true orbit
92 and provide analytical results to validate the numerical compu-
93 tations. The statistical analysis of actual roundoff errors is
94 postponed to a forthcoming paper.

95 We consider a class \mathcal{M} of dynamical systems with
96 strong mixing properties (see Sec. II for a rigorous defini-
97 tion) for which exact results are proved and integrable dy-
98 namical systems as well. The error induced by a random
99 perturbation of the map T in the computation of a smooth
100 observable f is defined by

$$101 \quad \Delta_n^\varepsilon = f(T^n x) - f(T_{\omega_n}^n x), \quad (1)$$

102 where $T_{\omega}^n = T_{\omega_1} \circ \dots \circ T_{\omega_n}$, $|\omega_i| \leq \varepsilon$. This random variable is
103 taken with respect to the probability measure given by the
104 direct product of the Lebesgue measure m over X and the
105 measure $\theta_\varepsilon^{\mathbb{N}}$ (see Sec. II) over the space of the realizations ω .
106 The characteristic function φ_n^ε of the random variable Δ_n^ε is
107 simply related to the *random* classical fidelity, introduced in
108 Ref. 9, which is suited to investigate the statistics of the
109 asymptotic error since it converges pointwise to

$$110 \quad \varphi_n^\varepsilon(u) \rightarrow \mathbb{E}_\mu(e^{ifu}) \overline{\mathbb{E}_{\mu_\varepsilon}(e^{ifu})}, \quad (2)$$

111 where the expectation values are calculated with respect to
112 the invariant measure μ of the map T and to the stationary
113 measure μ_ε of the stochastic perturbation T_ε of the map T
114 (the bar denotes complex conjugation, see details in Sec. II).
115 We show that this convergence is exponential with a rate
116 which is related to the rate of decay of correlations. The
117 left-hand side of Eq. (2) is the characteristic function of a
118 random variable which we interpret as the *asymptotic error*
119 and denote with $\Delta_\infty^\varepsilon$. This is the main quantity investigated in
120 this paper.

121 The asymptotic error can be computed not only for cha-
122 otic maps but also for regular maps such as rotations. For the
123 Bernoulli maps of the torus $qx \bmod 1$ and for rotations, a
124 complete analytical study, providing detailed information
125 about the transient to the asymptotic distribution, is possible.

126 Since the asymptotic error is the same for these proto-
127 types of regular and chaotic maps, the difference must be
128 searched for the transient, which reflects the divergence rate
129 of nearby unperturbed orbits. In particular the asymptotic
130 error is reached superexponentially fast for the Bernoulli
131 map and just exponentially fast for rotations; in the first case
132 the transition is very sharp, whereas it is smooth in the sec-
133 ond case. The time scales for the convergence to the
134 asymptotic error distribution are $n \sim \log(1/\varepsilon)$ and $n = \varepsilon^{-2}$, re-
135 spectively. We also investigate, mostly numerically, systems
136 with “intermediate” ergodic properties, such as intermittent
137 maps, the logistic map, the Hénon attractor, and the standard
138 map.

139 The plan of the paper is the following. Section II is
140 devoted to analytical results for the class \mathcal{M} . In Sec. III we

present the analytical results on two prototypes of regular
and chaotic maps and compare them with numerical compu-
tations. In Sec. IV we present the results of numerical compu-
tations for several systems, where analytical results are
missing: in particular we consider fractal attractors and fol-
low the evolution looking at observables with a Cantorian
structure. For these systems also the density distribution
function for the asymptotic error has a fractal shape. Our
major achievements are summarized in Sec. V and technical
details are explained in Appendices A–D.

II. ERROR STATISTICS

A. Random perturbations and fidelity

Let X be a compact Riemannian manifold equipped with
the Lebesgue measure m and consider a Borel measurable
map $T: X \rightarrow X$ admitting a physical measure μ (very often
also called SRB measure from Sinai, Ruelle, and Bowen who
introduced it), which is defined through the limit

$$\lim_{n \rightarrow \infty} \int \psi \circ T^n dm = \int \psi d\mu, \quad (3)$$

where ψ is any continuous function over X . We introduce the
random perturbation of the preceding system and succes-
sively we consider the fidelity as an interesting quantity to
characterize the annealed correlation integrals arising under
the stochastic perturbation.

Let $(\omega_k)_{k \in \mathbb{N}}$ be a sequence of independent and identically
distributed (iid) random variables with values in the vector
space Ω_ε and with distribution θ_ε . To each $\omega \in \Omega_\varepsilon$ we asso-
ciate a map T_ω with $T_0 = T$ and define the iterated perturbed
map as $T_{\omega_n} \circ \dots \circ T_{\omega_1} \equiv T_\omega^n$.

According to Ref. 9 we consider a class of maps \mathcal{M} such
that the following are taken into account.

- (i) The iterated perturbed map admits an invariant sta-
tionary measure μ_ε defined by

$$\lim_{n \rightarrow \infty} \int_X \int_{\Omega_\varepsilon^{\mathbb{N}}} \psi(T_\omega^n x) d\theta_\varepsilon^{\mathbb{N}}(\omega) dm(x) = \int \psi d\mu_\varepsilon. \quad (4)$$

The distribution θ_ε is chosen in such a way that μ_ε
will be absolutely continuous with respect to m (see
Sec. II B), and moreover $\int_X \psi d\mu_\varepsilon \rightarrow \int_X \psi d\mu$ when
 $\varepsilon \rightarrow 0$ (stochastic stability).

- (ii) The correlation integral decays exponentially on the
space of \mathcal{C}^1 observables, i.e.,

$$\left| \int_X \psi_1(T^n x) \psi_2(x) dm(x) - \int_X \psi_1 d\mu \int_X \psi_2 d\mu \right| \leq C \lambda^{-n} \|\psi_1\|_1 \|\psi_2\|_2, \quad (5)$$

where $C > 0$ and $\lambda > 1$ are determined only by the
map T and the two norms depend on the map and on
the space of observables (Ref. 9).

- (iii) An exponential decay for the annealed correlation in-
tegral is assumed still for \mathcal{C}^1 functions,

$$\begin{aligned}
& \left| \int_X \int_{\Omega_\varepsilon^N} \psi_1(T_\omega^n x) \psi_2(x) d\theta_\varepsilon^N(\omega) dm(x) \right. \\
& \quad \left. - \int_X \psi_1 d\mu_\varepsilon \int_X \psi_2 dm \right| \\
& \leq C \lambda^{-n} \|\psi_1\|_1 \|\psi_2\|_2,
\end{aligned} \tag{6}$$

where C , λ , and the norms 1 and 2 are the same as in Eq. (5).

We introduce the *classical fidelity* by means of the following integral (this definition was inspired by Ref. 10):

$$F_n^\varepsilon = \int_X \int_{\Omega_\varepsilon^N} \psi_1(T_\omega^n x) \psi_2(T_\omega^n x) d\theta_\varepsilon^N(\omega) dm(x), \tag{7}$$

where ψ_1 and ψ_2 are C^1 functions.

It is possible to prove the following theorem (Ref. 9).

Theorem 1: For the class \mathcal{M} there exists a constant $C_1 > 0$ for which

$$\begin{aligned}
& \left| F_n^\varepsilon - \int_X \psi_1 d\mu_\varepsilon \int_X \psi_2 d\mu \right| \\
& \leq C_1 \varepsilon^{-\kappa} \lambda^{-n} (\|\psi_2\|_1 \|\psi_1\|_{C^0} + \|\psi_1\|_1 \|\psi_2\|_{C^0}),
\end{aligned} \tag{8}$$

where $\|\cdot\|_1$ is a suitable norm on the space of observables and $\|\cdot\|_{C^0}$ is the supremum norm on continuous functions.

B. Additive noise

In this article we restrict ourselves to a particular random perturbation, the additive noise, which satisfies the assumptions of Theorem 1 and is well defined whenever the space X is the d -dimensional torus $X = \mathbb{T}^d$. In this case we define the random maps as $T_\omega = Tx + \omega \bmod \mathbb{T}^d$, where $\omega \in \mathbb{T}^d$, and then take θ_ε absolutely continuous with respect to the Lebesgue measure $d\omega$ over \mathbb{T}^d and with a bounded density h_ε with support contained in the square $[-\varepsilon, \varepsilon]^d$ and such that $\int d\theta_\varepsilon = \int h_\varepsilon(\omega) d\omega = 1$. Letting $H(\xi)$ be a non-negative bounded function with support on $[-1, 1]^d \subset \mathbb{R}^d$ such that $\int H(\xi) d\xi = 1$, the function $h_\varepsilon(x)$ is defined by $h_\varepsilon(\omega) = \varepsilon^{-d} H(\omega/\varepsilon)$. The change in variable $\omega = \varepsilon\xi$ shows that the density $h_\varepsilon(\omega)$ of the measure $\theta_\varepsilon(\omega)$ has the required properties. For the maps of the torus \mathbb{T} discussed in Sec. III we consider a sequence of iid random variables $(\xi_k)_{k \in \mathbb{N}}$ in $[-1, 1] \subset \mathbb{R}$ and a function $H(\xi)$ equal to $1/2$ for $|\xi| \leq 1$ and equal to 0 for $|\xi| > 1$, limit of a sequence of normalized functions with support in $\xi \in [-1, 1]$. As a consequence after the change $\omega = \varepsilon\xi$ the fidelity we compute reads

$$F_n^\varepsilon = 2^{-d} \int_0^1 dx \int_{-1}^1 d\xi \psi_1(T^n x) \psi_2(T_{\varepsilon\xi_n} \circ \dots \circ T_{\varepsilon\xi_1} x). \tag{9}$$

When the phase space X is a subset $D \in \mathbb{R}^n$, we require that the image of D is strictly included in D and that it remains so when randomly perturbed. It is straightforward to check that the orbits generated by maps perturbed with additive noise are ε pseudo-orbits. The equivalence between pseudo-orbits and random orbits holds for a wider class of noises, see Ref. 11.

Remark 1: Reference 9 gives several examples of dynamical systems satisfying Theorem 1: Anosov diffeomorphisms, uniformly hyperbolic attractors, piecewise expanding maps of the interval, and uniformly hyperbolic maps with singularities. Theorem 1 could be generalized by considering two randomly iterated perturbed maps T_ω^n and $T_{\omega'}^n$ having stationary measures μ_ε and μ'_ε . Equation (8), where we replace T^n with $T_{\omega'}^n$ and μ with μ'_ε , would still hold. This result allows us to compare a randomly perturbed map with another one having a smaller perturbation when the exact map is not available as it happens in numerical computations.

C. Error distribution

We consider the dynamical system (X, T, μ) , where μ is a physical measure, and the family of random transformations T_{ω_k} previously defined. Let $f: X \rightarrow \mathbb{R}$ be a C^1 observable and $m \otimes \theta_\varepsilon^N$ be the probability measure on the product space $X \times \Omega_\varepsilon^N$. The basic quantity investigated in this paper is the algebraic error

$$\Delta_n^\varepsilon = f(T^n x) - f(T_\omega^n x) \tag{9}$$

given by the difference of two stochastic processes, for which we now state the following result that we use to investigate asymptotic distributions of errors.

Theorem 2: Suppose the map $T \in \mathcal{M}$; then when n goes to $+\infty$, the random process Δ_n^ε , whose characteristic function is $\varphi_n^\varepsilon(u)$, converges in distribution to a random variable $\Delta_\infty^\varepsilon$ whose characteristic function is given by

$$\varphi_\infty^\varepsilon(u) = \lim_{n \rightarrow \infty} \varphi_n^\varepsilon(u) = \int_X e^{iuf} d\mu \int_X e^{-iuf} d\mu_\varepsilon. \tag{10}$$

Proof: Indeed writing the characteristic function of the variable Δ_n^ε as $\varphi_n^\varepsilon(u)$ and using Fubini theorem, we have

$$\begin{aligned}
\varphi_n^\varepsilon(u) & \equiv \int_{X \times \Omega_\varepsilon^N} e^{iu\Delta_n^\varepsilon(x, \omega)} dm(x) d\theta_\varepsilon^N(\omega) \\
& = \int_X \int_{\Omega_\varepsilon^N} e^{iu[f(T^n x) - f(T_\omega^n x)]} d\theta_\varepsilon^N(\omega) dm(x).
\end{aligned} \tag{10}$$

By Theorem 1 and by choosing $\psi_1(x) = e^{iuf(x)}$, $\psi_2(x) = e^{-iuf(x)}$ we immediately get the equality (10). Let us now denote with Φ_n^ε the distribution function of the variable Δ_n^ε ; if we can prove that $\varphi_\infty^\varepsilon$ is continuous at $u=0$, then by Theorem 3, p. 266 in Ref. 12, we can conclude that $\varphi_\infty^\varepsilon$ is the characteristic function of some distribution function Φ_∞^ε and Φ_n^ε converges *completely* to Φ_∞^ε . In this case we will say that the random variables Δ_n^ε converge in *distribution* or *law* to a random variable, which we denote with $\Delta_\infty^\varepsilon$ and which has Φ_∞^ε as distribution function.

Since $|e^{\pm iuf}| \leq 1$ and μ and μ_ε are probability measures, by the dominated convergence theorem we immediately have that $\lim_{u \rightarrow 0} \varphi_\infty^\varepsilon(u) = 1 = \varphi_\infty^\varepsilon(0)$, which proves that $\varphi_\infty^\varepsilon$ is continuous at 0.

We are not really interested in the random variable $\Delta_\infty^\varepsilon$, but rather in its distribution function Φ_∞^ε . Whenever $\int_{-\infty}^{\infty} |\varphi_\infty^\varepsilon(u)| du < \infty$, the Lévy inversion formula asserts that the

279 distribution function Φ_∞^ε is absolutely continuous with a
 280 bounded continuous density ρ_∞^ε [probability density function
 281 (pdf)] given by

$$\rho_\infty^\varepsilon(t) = \frac{1}{2\pi} \int_{-\infty}^{\infty} e^{-iut} \varphi_\infty^\varepsilon(u) du. \quad (11)$$

283 We also note that the convergence to the asymptotic charac-
 284 teristic function is exponential but not uniform in the noise

$$|\varphi_n^\varepsilon(u) - \varphi_\infty^\varepsilon(u)| = \mathcal{O}(\varepsilon^{-\kappa} \lambda^{-n}). \quad (12)$$

286 This point is further investigated in Secs. III and IV and in
 287 Appendix D.

288 *Remark 2: Since our random variable Δ_n^ε is bounded on*
 289 *X , all its moments are uniformly integrable and the moments*
 290 *of $\Delta_\infty^\varepsilon$ are given by the limit, for $n \rightarrow \infty$, of the corresponding*
 291 *moments of Δ_n^ε . In particular, we have*

$$(i) \quad \mathbb{E}_{m \otimes \theta_\varepsilon^N}(\Delta_\infty^\varepsilon) = \mathbb{E}_\mu(f) - \mathbb{E}_{\mu_\varepsilon}(f),$$

$$(ii) \quad \mathbb{V}_{m \otimes \theta_\varepsilon^N}(\Delta_\infty^\varepsilon) = \mathbb{V}_\mu(f) + \mathbb{V}_{\mu_\varepsilon}(f)$$

$$= \int f^2 d\mu - \left(\int f d\mu \right)^2 + \int f^2 d\mu_\varepsilon - \left(\int f d\mu_\varepsilon \right)^2,$$

296 where \mathbb{E}_ν (respectively \mathbb{V}_ν) denotes the expectation (respec-
 297 tively the variance) with respect to the measure ν . Since we
 298 have assumed $\mu_\varepsilon \rightarrow \mu$ (stochastic stability), the average of
 299 the asymptotic error vanishes when $\varepsilon \rightarrow 0$, whereas its vari-
 300 ance remains finite. This is a memory phenomenon because
 301 even if the noise vanishes after the system has evolved its
 302 effect persists. This is another consequence of the stochastic
 303 instability of the classical fidelity pointed out in Ref. 9. Ad-
 304 ditional considerations may be found in Appendix A, where
 305 we compare our results with a recent related work by Sauer.

306 III. ANALYTICAL RESULTS ON PROTOTYPE 307 MAPS

308 A. Chaotic maps and rotations on the circle

309 As an easy illustration of the theorem 2 we consider the
 310 map T defined on one-dimensional (1D) torus $X = \mathbb{T}^1$ by Tx
 311 $= qx \bmod 1$, where $q \geq 2$ is a positive integer. We perturb it
 312 with additive noise producing the random transformations
 313 $T_{\varepsilon\xi}(x) = qx + \varepsilon\xi \bmod 1$, where $\varepsilon > 0$ is the noise intensity and
 314 ξ is a random variable uniformly distributed over $[-1, 1]$. By
 315 inspection of formula (4), it is easy to check that the noise
 316 just introduced has a stationary measure which coincides
 317 with the Lebesgue measure on \mathbb{T}^1 . The map T clearly belongs
 318 to \mathcal{M} and theorem 2 holds for smooth observables. We shall
 319 rather consider the observable *identity* $f(x) = x$ which is dis-
 320 continuous on the torus. A direct proof of convergence will
 321 be given by using Fourier series, and we show in Sec. III B
 322 that the characteristic function of the asymptotic error is
 323 $\varphi_\infty^\varepsilon(u) = 2u^{-2}(1 - \cos u)$ [in agreement with Eq. (2)]. The
 324 asymptotic error is the triangular function on $[-1, 1]$, namely,
 325 $\rho_\infty^\varepsilon(t) = (1 - |t|) \mathbb{1}_{[-1, 1]}$.

We apply the same Fourier analysis to regular maps, such as the translations on the torus $Tx = x + \chi \bmod 1$, which correspond to rotations of angle $2\pi\chi$ on the circle \mathbb{C}^1 , and we perturb it with additive noise [we stress that for such maps our theorem 2 does not apply]. The random map iterated n times reads

$$T_{\varepsilon\xi}^n \equiv x + n\chi + \varepsilon(\xi_1 + \xi_2 + \dots + \xi_n) \bmod 1, \quad (13)$$

where the $(\xi_l)_{l \geq 1}$ are iid random variables with common uniform distribution over $[-1, 1]$. The Lebesgue measure on \mathbb{T}^1 is the unique stationary measure for the process. Let us consider the fidelity [Eq. (9)] F_n^ε for the function $\psi = \psi_1 = \psi_2^*$ with Fourier coefficients $(\psi_k)_{k \in \mathbb{Z}}$. The function ψ is taken piecewise C^1 (at least) with a finite number of discontinuity points. Simple calculations give (see Appendix B)

$$F_n^\varepsilon = |\psi_0|^2 + \sum_{k \neq 0} |\psi_k|^2 S^n(k\varepsilon), \quad S(x) = \frac{\sin(2\pi x)}{2\pi x}. \quad (14)$$

The function S can be bounded by

$$|S(x)| \leq \begin{cases} e^{-\ln(2\pi)x^2} & \text{if } |x| < 1 \\ \frac{1}{2\pi|x|} & \text{if } |x| \geq 1. \end{cases} \quad (15)$$

Using this bound in Eq. (14) and since the Fourier coefficients are at least bounded by $|\psi_k| \leq C|k|^{-1}$, where C is a constant depending on the observable ψ , we get, after a few manipulations (see Appendix B for details),

$$|F_n^\varepsilon - |\psi_0|^2| \leq C^2((2 - \varepsilon)e^{-\varepsilon^2 n \ln(2\pi)} + 2\varepsilon(2\pi)^{-n}). \quad (16)$$

This result applies also to $\varphi_n^\varepsilon(u)$, which is the fidelity computed using $\psi = e^{iuf(x)}$.

B. Transients for the maps on the torus

Since Eq. (16) converges to zero and by taking $f(x) = x$, the asymptotic distribution of errors $\Delta_\infty^\varepsilon$ for rotations is again the triangular distribution, as in the case of $qx \bmod 1$ with $q \geq 2$. Therefore a chaotic and a very regular map (which is the identity for $\chi = 0$) share the same distribution for the error between the true orbit and its random perturbation with the same initial condition. This is not surprising if one realizes that what we are doing for the observable identity $f(x) = x$ is just to compute the distribution of the difference of two points selected randomly, and independently one from the other, on the circle with uniform distribution: the distribution of the difference is just the triangular law. The previous required statistical assumptions are guaranteed by the Bernoulli property of the map $qx \bmod 1$ and by the independence and the common uniform distribution of the kicks ξ_l for rotations.

The very different ergodic properties of the two systems are reflected, however, in the rate of convergence to the limiting distribution. Equation (12) suggests an exponential decay for \mathcal{M} maps [for $qx \bmod 1$ the exponent is $\kappa = 1$ (Ref. 9)], but we can considerably improve the latter estimate using Fourier series and prove that the convergence for $qx \bmod 1$ is indeed superexponential. We first observe that

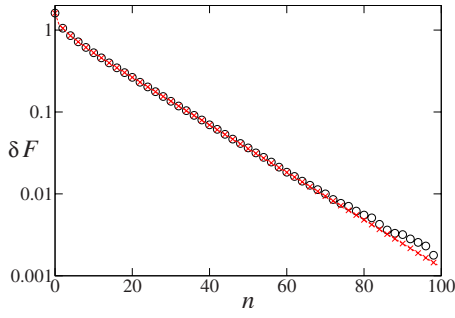


FIG. 1. (Color online) Comparison between the analytical result, Eq. (14), and Monte Carlo integrals for the decay of fidelity [Eq. (24)] in rotations, $\varepsilon=0.1$ (analytical result: red dashed line and crosses; Monte Carlo: circles). We used $N=10^7$ integration points in the Monte Carlo method. The test functions $\psi_1=\psi_2^*$ were defined in Fourier space as $\psi_k=k^{-1}$ truncated at $k=30$.

$$F_n^\varepsilon = |\psi_0|^2 + \sum_{k \neq 0} |\psi_k|^2 S_{n,q}(k\varepsilon), \quad (17)$$

where we have defined

$$S_{n,q}(x) = \prod_{k=0}^{k=n-1} S(q^k x) \quad (18)$$

(the proof of this equation is given in Appendix B). A bound for Eq. (17) can be found as

$$|F_n^\varepsilon - |\psi_0|^2| \leq \begin{cases} Ae^{-\alpha q^{2(n-n_*)}} & \text{if } n < n_* \\ Ae^{-\alpha q^{-(n-n_*)^2/2}} & \text{if } n \geq n_*, \end{cases} \quad (19)$$

where

$$\varepsilon q^{n_*} = 1 \quad \text{or} \quad n_* = -\log_q \varepsilon. \quad (20)$$

This formula shows a sharp transition in the decay whenever $n \sim \ln \varepsilon^{-1} / \ln q = n_*$ and the decay becomes superexponential. Instead, for rotations, such a transition point does not exist and the decay is smooth, see Figs. 1 and 2. The difference between these two regimes becomes also apparent when we compute ρ_n^ε , the distribution function of Δ_n^ε , for the identity observable, which is given by the inverse Fourier transform of the following characteristic functions that we obtain after evaluating the Fourier coefficients

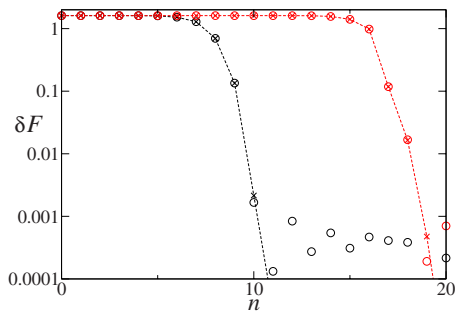


FIG. 2. (Color online) Comparison between the analytical result, Eq. (17), and Monte Carlo integral for the decay of fidelity [Eq. (24)] in $3x \bmod 1$. $\varepsilon=10^{-4}$ in black and $\varepsilon=10^{-8}$ in red (gray in black and white) (analytical result: dashed line and crosses; Monte Carlo: circles). We used $N=10^7$ integration points in the Monte Carlo method. The test functions $\psi_1=\psi_2^*$ were defined in Fourier space as $\psi_k=k^{-1}$ truncated at $n=30$.

$$\psi_k = e^{i(u/2 - \pi k)} \frac{\sin(u/2 - \pi k)}{u/2 - \pi k} \quad 391$$

of the function $\psi(x)$ defined on the torus so that $\psi(x)=e^{iux}$ for $0 \leq x < 1$, namely,

$$\psi(x) = \begin{cases} e^{iu(x-[x])} & \text{if } x > 0 \\ e^{iu(1+x-[x])} & \text{if } x < 0, \end{cases} \quad (21) \quad 394$$

where $[x]$ stands for the integer part of $x \in \mathbb{R}$ (this choice is equivalent to study e^{iux} defined on the torus). The result explicitly reads

$$\varphi_n^\varepsilon(u) = \frac{2}{u^2}(1 - \cos u) + \sum_{k=1}^{\infty} S^n(k) \left[\frac{\sin^2(u/2 - \pi k)}{(u/2 - \pi k)^2} + \frac{\sin^2(u/2 + \pi k)}{(u/2 + \pi k)^2} \right] \quad (22) \quad 398$$

for rotations and

$$\varphi_n^\varepsilon(u) = \frac{2}{u^2}(1 - \cos u) + \sum_{k=1}^{\infty} S_{n,q}(k) \left[\frac{\sin^2(u/2 - \pi k)}{(u/2 - \pi k)^2} + \frac{\sin^2(u/2 + \pi k)}{(u/2 + \pi k)^2} \right] \quad (23) \quad 401$$

for $qx \bmod 1$. See Appendix B for more details. The inverse Fourier transform of $2u^{-2}(1 - \cos u)$ is the triangular distribution so that

$$\rho_\infty^\varepsilon(t) = (1 - |t|) \mathbb{1}_{[-1,1]}. \quad 406$$

The continuum limit of these processes is described in Appendix C.

C. Comparison to numerical results

We have compared the analytical results with the output of numerical computations based essentially on Eq. (9). The decay of fidelity [see also Eq. (8)] on $X=[0, 1]$ is defined by

$$\delta F_n^\varepsilon = F_n^\varepsilon - 2^{-d} \left(\int_0^1 dx \psi_1(T^n(x)) \right) \times \left(\int_0^1 dx \int_{-1}^1 d\xi \psi_2(T_{\varepsilon\xi_n} \circ \dots \circ T_{\varepsilon\xi_1} x) \right), \quad (24) \quad 413$$

where F_n^ε is given by Eq. (9). The integrals are performed randomly choosing N vectors (x, ξ) in $\mathbb{R}^{d(n+1)}$, i.e., using a Monte Carlo method whose accuracy is of order $N^{-1/2}$. For smooth test functions, integration methods with regularly distributed x points can improve the accuracy, but since for chaotic maps the smoothness of the integrand is rapidly lost and integration error estimates are difficult we systematically use a Monte Carlo on (x, ξ) for which the error estimate $N^{-1/2}$ always holds. We show the comparison between the analytical and numerical results on the decay of fidelity for rotations (Fig. 1) and for the map $3x \bmod 1$ (Fig. 2); while in Figs. 3–6 we compare the analytical results for ρ_n^ε [Fourier inversion of Eqs. (22) and (23)] with the corresponding numerical computations (i.e., with a Monte Carlo sampling of the error Δ_n^ε in which the probability function ρ_n^ε is approxi-

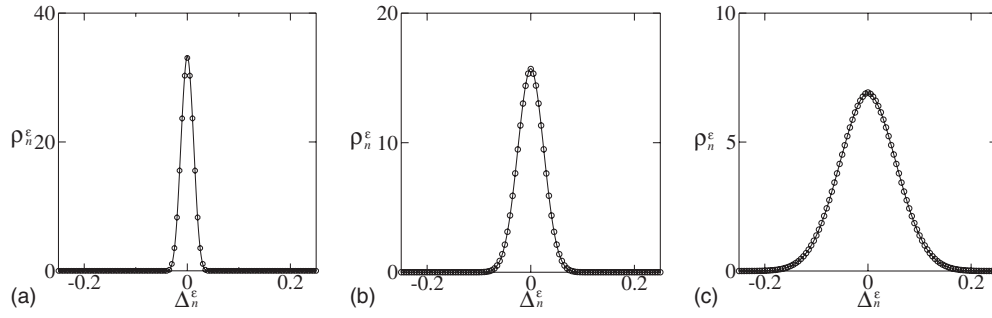


FIG. 3. Comparison between the analytical result for ρ_n^ε in rotations, Fourier transform of Eq. (22) (continuous line), and Monte Carlo sampling (circles), $\varepsilon=10^{-2}$. (a) $n=4$; (b) $n=19$; (c) $n=99$.

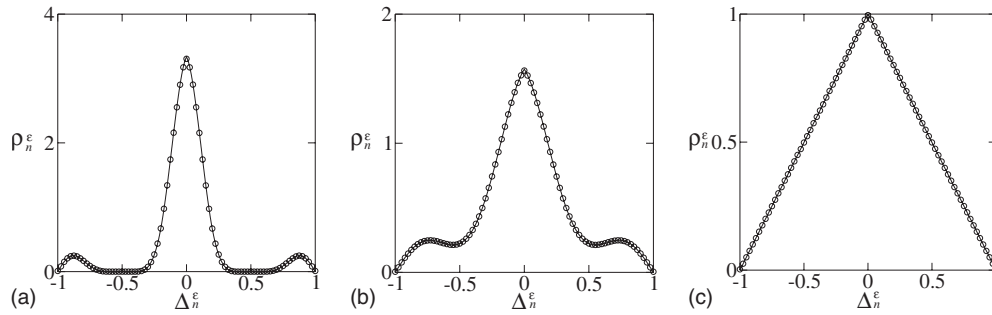


FIG. 4. Comparison between the analytical result for ρ_n^ε in rotations, Fourier transform of Eq. (22) (continuous line), and Monte Carlo sampling (circles), $\varepsilon=0.1$. (a) $n=4$; (b) $n=19$; (c) $n=99$. Compare the transition times with Fig. 1.

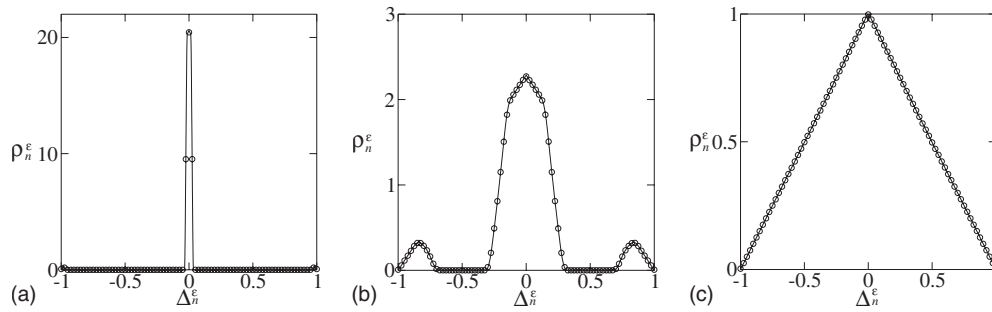


FIG. 5. Comparison between the analytical result for ρ_n^ε in $3x \bmod 1$, Fourier transform of Eq. (23) (continuous line), and Monte Carlo sampling (circles), $\varepsilon=10^{-4}$. (a) $n=6$; (b) $n=8$; (c) $n=10$. Compare the transition times with Fig. 2.

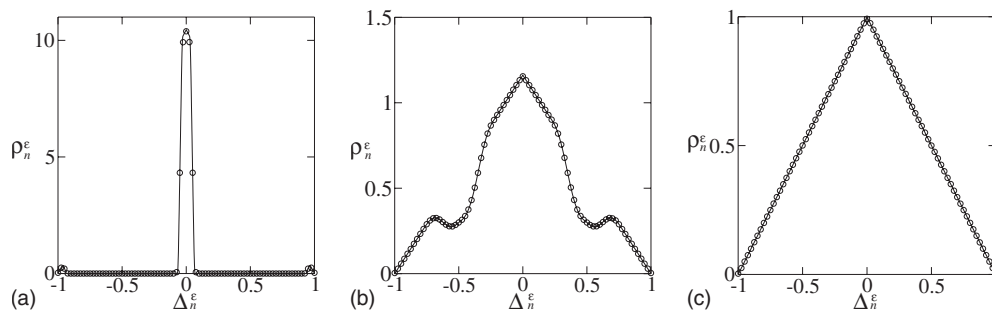


FIG. 6. Comparison between the analytical result for ρ_n^ε in $3x \bmod 1$, Fourier transform of Eq. (23) (continuous line), and Monte Carlo sampling (circles), $\varepsilon=10^{-8}$. (a) $n=15$; (b) $n=17$; (c) $n=19$. Compare the transition times with Fig. 2.

430 mated by the probability of Δ_n^ε to be in an interval of length
431 Δx).

432 These figures show clearly that while for rotations the
433 transition from the initial condition $\rho_0^\varepsilon(x)=\delta(x)$ to the
434 asymptotic (triangular) distribution is a gradual process,
435 whose time scale is of order ε^{-2} , for the map $3x \bmod 1$ we
436 have a sharp transition that starts around $n_*=-\log_q \varepsilon$ [see
437 Eq. (19)]. In the transition region the slope does not depend
438 on ε but is related to the divergence of nearby orbits, namely,
439 to the decay rate of correlations λ or the maximum Lyapunov
440 exponent Λ (for several systems $\lambda=e^\Lambda$). According to
441 Eq. (20) when ε varies from 10^{-4} to 10^{-8} the transition n_*
442 varies by a factor of 2. For $n \ll n_*$ the error distribution func-
443 tion can be well approximated by a δ function, i.e., the per-
444 turbed system can be considered as equivalent to the unper-
445 turbed one.

446 In both regular and chaotic maps the asymptotic distri-
447 bution is reached when δF_n approaches a value a few order
448 of magnitude lower than the initial value. We remark that
449 $\rho_n^\varepsilon(x)$ is the Fourier transform of $\varphi_n^\varepsilon(u)$, i.e., of the fidelity
450 computed using $\psi_1=\psi_2^*=e^{iux}$. The comparison between the
451 results in Figs. 1 and 2 and those in Figs. 3–6 suggests (as
452 we have verified analyzing different test functions) that the
453 decay of fidelity depends very weakly on the functions ψ_1 ,
454 ψ_2 , and thus that the analysis of a single, easily computable
455 test function provides information about the evolution of
456 $\rho_n^\varepsilon(x)$.

457 IV. NUMERICAL COMPUTATIONS

458 In this section we apply the theory developed above to
459 various dynamical systems; for the majority of them it is not
460 known whether all the conditions required to belong to the
461 class \mathcal{M} are satisfied. We compute numerically the distribu-
462 tion of the error ρ_n^ε for additive noise. The chosen observ-
463 ables are $f(x)=x$ for 1D maps and $f(\mathbf{x})=x$, $f(\mathbf{x})=y$ for two-
464 dimensional (2D) maps. Whenever x parametrizes a linear
465 subspace S of \mathbb{R} , the difference x_1-x_2 is the distance between
466 x_1 and x_2 up to a sign. The integrals with respect to the
467 physical measure and the stationary measure are performed
468 by using their definition as weak limits of the Lebesgue mea-
469 sure. These limiting measures are no longer equal to the
470 Lebesgue measure as in the examples in Sec. III. Two rel-
471 evant classes of maps are considered. In the first one, which
472 includes the maps with neutral fixed point(s) and the logistic
473 map, the measures are absolutely continuous with respect to
474 Lebesgue. In the second class, which includes the Hénon and
475 the Baker's maps, the invariant measures are singular with
476 respect to Lebesgue. For these maps the attractor has a frac-
477 tal structure, which is locally described as the product of a
478 smooth manifold with a Cantor set. When we deal with maps
479 which are not hyperbolic and admit an absolutely continuous
480 invariant measure with a density which is summable but not
481 necessarily bounded (this is notably the case of the intermit-
482 tent and quadratic maps), or when we have singular invariant
483 measures as for the Hénon and the Baker's maps, we are not
484 anymore sure that the characteristic function $\varphi_\infty^\varepsilon$ is Lebesgue

integrable. We remind that this is a sufficient condition in
order to apply the Lévy inversion formula (11). In Appendix
D we explain what happens when we lose the summability of
the characteristic function.

The numerical analysis consists of four steps.

- Decay of fidelity in a test function. On the basis of the results obtained for translations on the torus and for the map $qx \bmod 1$, we study the decay of fidelity [Eq. (24)] for the test function $\psi(x)=x$ (x observable) using a Monte Carlo method to compute the integrals. This analysis provides the values of n at which the transition from $\rho_0^\varepsilon = \delta(x)$ to the asymptotic regime ρ_∞^ε occurs.
- Computation of ρ_n^ε for significant values of n . Using a Monte Carlo sampling we perform the statistical analysis of Δ_n^ε , estimating its distribution ρ_n^ε , for the values of n suggested by the analysis in the first step.
- Asymptotic limit. The two previous steps allow us to identify a value $\bar{n}(\varepsilon)$ beyond which ρ_n^ε has reached its asymptotic value. We thus compute with high accuracy ρ_∞^ε as the average $\bar{\rho}_n^\varepsilon$ over several values $n' > \bar{n}$.
- Check of the validity of Eq. (2). We compute $\varphi_\infty^\varepsilon$ using Eq. (2), and its Fourier transform, to check if it coincides with ρ_∞^ε that is computed with a Monte Carlo sampling, as predicted by Theorem 2.

Remark 3: In numerical computations, we cannot evaluate the error $\Delta_n^\varepsilon=f(T^n x)-f(T_\omega^n x)$. In fact both T and T_ω are affected by the arithmetic roundoff, which in a single step introduces an error of order ε_{num} . The orbit T^n is replaced by the perturbed orbit $T_{\omega'}^n$, where ω'_i are now "random" variables in the space, say, $\Omega_{\varepsilon_{\text{num}}}(0)$ around the unperturbed component 0. In the same way the random orbit T_ω^n will be replaced by a new random orbit $T_{\omega''}^n$, where the components ω''_i are now random variables in the space $\Omega_{\varepsilon_{\text{num}}}(\omega_1)$ around the component ω_1 . Comparing $\Delta_n^{\varepsilon, \varepsilon_{\text{num}}}=f(T_{\omega'}^n x)-f(T_{\omega''}^n x)$ with the analytical estimate for Δ_n^ε , or just letting $\varepsilon_{\text{num}} \rightarrow 0$ by using arbitrary precision arithmetic, we can check that if $\varepsilon \gg \varepsilon_{\text{num}}$, there is a time scale relevant for the study of Δ_n^ε , below which the additional error $\Delta_n^\varepsilon - \Delta_n^{\varepsilon, \varepsilon_{\text{num}}}$ is negligible with respect to Δ_n^ε . Since the numerical roundoff error in double precision for a variable on the torus is of order $\varepsilon_{\text{num}} \approx 10^{-16}$, we are going to use additive noise $\varepsilon > 10^{-9}$. The choice $\varepsilon \approx 10^{-8}$, corresponding to single precision numerical roundoff, is of interest for future investigations on the statistics of roundoff errors in the iteration of maps. The convergence in distribution of the process $\Delta_n^{\varepsilon, \varepsilon}$ is guaranteed by the generalization of Theorem 1 provided in Remark 1. We observe that Sauer in Ref. 13 faced the same problem in developing a theory of true and perturbed orbits while checking the predictions of computer experiments. He wrote, "We computed the trajectory average in high precision (used to represent the "true" value) for a long trajectory and compared it with the trajectory computed with one-step random error of size ε ."

A. Hénon map

The Hénon map is a 2D map defined by

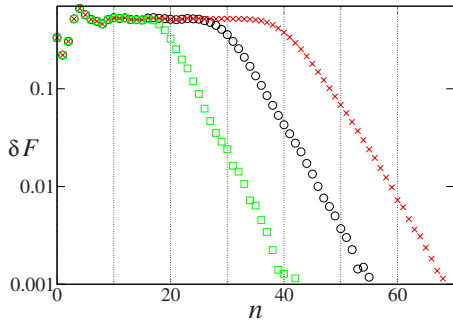


FIG. 7. (Color online) Decay of fidelity for the Hénon map, Monte Carlo integration with $N=10^7$. Green squares: $\varepsilon=10^{-4}$. Black circles: $\varepsilon=10^{-6}$. Red crosses: $\varepsilon=10^{-8}$.

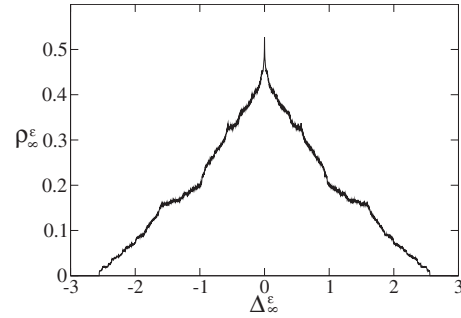


FIG. 9. ρ_∞^ε for the Hénon map with $\varepsilon=10^{-8}$, $f(\mathbf{x})=x$ given by the average of 10^6 samplings of ρ_n^ε , each one obtained using a Monte Carlo method with 10^3 starting points ($N=10^9$) and $\Delta x=10^{-3}$.

540
$$T\mathbf{x} = \begin{cases} x' = y + 1 - ax^2 \\ y' = bx. \end{cases} \quad (25)$$

541 We consider the canonical values $a=1.4$ and $b=0.3$, for
 542 which the map is known to be chaotic, at least numerically.
 543 We remind that Benedicks and Carleson¹⁴ proved that there
 544 exists a set of positive Lebesgue measure S in the parameter
 545 space such that the Hénon map has a strange attractor when-
 546 ever $(a, b) \in S$. The value of b is very small and the attractor
 547 lives in a small neighborhood of the x -axis. For those values
 548 of a and b , one can prove the existence of the physical mea-
 549 sure and of a stationary measure under additive noise, which
 550 is supported in the basin of attraction and that converges to
 551 the physical measure in the zero noise limit.¹⁵ It is still un-
 552 known whether such results could be extended to the “his-
 553 torical” values that we consider here.

554 The orbit starting at (x_0, y_0) will either approach the
 555 Hénon strange attractor or diverge to infinity. We study a
 556 connected subset D included in the basin of the attractor and
 557 define on it the perturbed map

558
$$T_{\varepsilon\xi}\mathbf{x} = \begin{cases} x' = y + 1 - ax^2 + \varepsilon\xi_x \\ y' = bx + \varepsilon\xi_y. \end{cases} \quad (26)$$

559 We have verified that using $D=(x, y)$ with $-1 < x < 1$ and
 560 $-1/2 < y < 1/4$ the set D is stable under small perturbations
 561 [i.e., the point (x_0, y_0) does not diverge to infinity under T_ε
 562 for small enough ε].

563 We studied the decay of fidelity [Eq. (24)] with observ-
 564 ables x and y . After a transient that depends on the definition
 565 of the set D , the fidelity reaches a plateau, and then follows
 566 a decay phase (Fig. 7), whose rate does not depend on ε . The

ε dependence is manifest in the outset of the decay (end of
 plateau). We name the value of n at which the decay phase
 starts n_* since its ε dependence is qualitatively compatible
 with Eq. (20). The height of the plateau, n_* , and the decay
 law are independent of the choice of D , as expected due to
 the ergodic properties of the map. The behavior of the y
 observable is almost the same as that of x . We successfully
 checked (Fig. 8) that the transition from $\rho_0^\varepsilon = \delta(x)$ to the
 asymptotic ρ_∞^ε starts with the outset of the decay phase of the
 fidelity (for example, around $n_* \approx 35$ in Fig. 7 for $\varepsilon=10^{-8}$).
 Below this time scale the error distribution function can be
 approximated by a δ function and thus the perturbed system
 can be considered as equivalent to the unperturbed one. We
 finally averaged ρ_n^ε over several $n > n_*$ in order to obtain ρ_∞^ε
 (Fig. 9) and checked, with good results, the validity of
 Eq. (2).

B. Baker’s map

The Baker’s map is defined by $T\mathbf{x}=\mathbf{x}'$, where

$$x' = \begin{cases} \gamma_\alpha x \bmod 1 & \text{if } y < \alpha \\ \frac{1}{2} + \gamma_\beta x \bmod 1 & \text{if } y \geq \alpha, \end{cases}$$

$$y' = \begin{cases} \frac{y}{\alpha} \bmod 1 & \text{if } y < \alpha \\ \frac{y - \alpha}{1 - \alpha} \bmod 1 & \text{if } y \geq \alpha, \end{cases}$$

while its perturbed version is

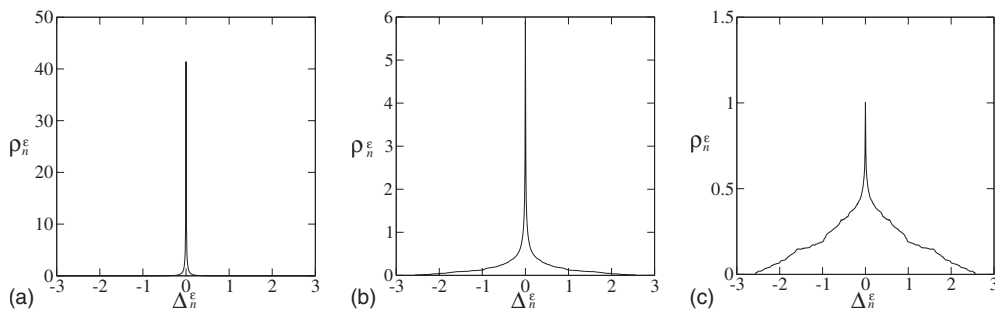


FIG. 8. ρ_n^ε for the Hénon map, $\varepsilon=10^{-8}$, $f(\mathbf{x})=x$. (a) $n=34$; (b) $n=44$; (c) $n=54$. Monte Carlo sampling using $N=10^8$ initial points and space discretization $\Delta x=10^{-2}$.

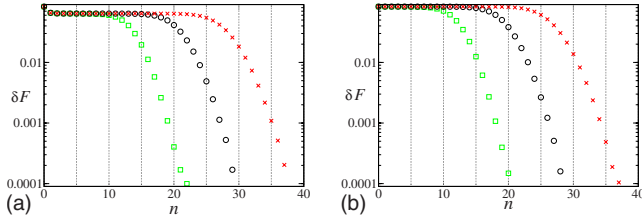


FIG. 10. (Color online) Decay of fidelity for the Baker's map. Monte Carlo integration with $N=10^7$. Green squares: $\varepsilon=10^{-4}$. Black circles: $\varepsilon=10^{-6}$. Red crosses: $\varepsilon=10^{-8}$. (a) x observable. (b) y observable.

$$588 \quad T_{\varepsilon\xi}\mathbf{x} = (x' + \varepsilon\xi_x \bmod 1, y' + \varepsilon\xi_y \bmod 1).$$

589 Using $\gamma_a = \frac{1}{5}$, $\gamma_b = \frac{1}{4}$, and $\alpha = \frac{1}{3}$ we studied the decay of fidelity
590 for the x and y observables (Fig. 10).

591 While the decay of fidelity for $\psi(\mathbf{x})=y$ shows a plateau
592 and then a decay phase, for $\psi(\mathbf{x})=x$ the plateau is preceded
593 by a decrease in the value of fidelity due to the convergence
594 to the invariant measure. The difference between the first
595 steps of fidelity for y and x is due to the different nature of
596 the invariant distributions (uniform for y and a Cantor set for
597 x); nevertheless the outset of fidelity decay (end of plateau)
598 happens roughly at the same n_* for the two observables
599 ($n_* \approx 20$ for $\varepsilon=10^{-8}$). Once again the ε dependence of n_* is
600 in agreement with Eq. (20), and it is followed by an ε inde-
601 pendent decay law. Also for this map the analysis of fidelity
602 predicts quite well the outset of the transient from a delta
603 function to the asymptotic distribution for the error distribu-
604 tion (not shown). While for $f(\mathbf{x})=y$, $\rho_\varepsilon^\varepsilon$ is simply the trian-
605 gular function, for the observable x we have a Cantor struc-
606 ture that can be better appreciated increasing the precision of
607 the computation (Fig. 11). We also checked that Eq. (2) holds
608 for this system. In order to understand the irregular shape of
609 the pdf for the observable x , we modify the Baker's map in
610 such a way to get the usual ternary Cantor set on the x -axis.
611 This can be easily achieved by writing the modified Baker's
612 map as

$$613 \quad x' = \begin{cases} \frac{x}{3} & \text{if } y < \frac{1}{2} \\ \frac{1}{2} + \frac{x}{3} & \text{if } y \geq \frac{1}{2}, \end{cases} \quad (27)$$

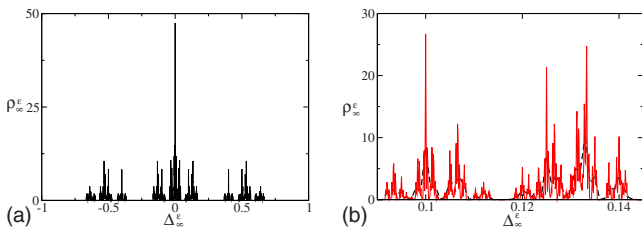


FIG. 11. (Color online) (a) ρ_x^ε for the Baker's map, $\varepsilon=10^{-8}$, x observable. Monte Carlo sampling using $N=10^9$ and $\Delta x=10^{-3}$. (b) detail of ρ_x^ε for the Baker's map, $\varepsilon=10^{-8}$, x observable. Black, dashed: Monte Carlo using $N=10^9$ and $\Delta x=10^{-3}$. Red, continuous: Monte Carlo using $N=10^{10}$ and $\Delta x=10^{-4}$.

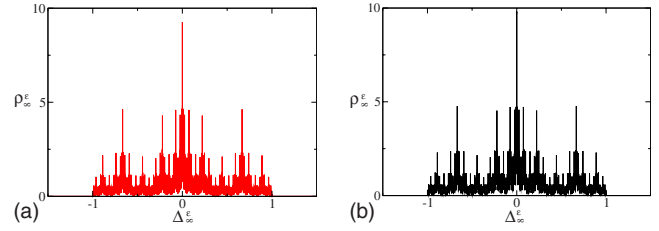


FIG. 12. (Color online) ρ_x^ε for the modified Baker map (whose invariant measure corresponds to a ternary Cantor set) as obtained by Eq. (28) (a) and by Monte Carlo method (b).

$$y' = \begin{cases} 2y & \text{if } y < \frac{1}{2} \\ 2y - 1 & \text{if } y \geq \frac{1}{2}. \end{cases} \quad 615$$

The physical SRB measure will be the direct product of an
absolutely continuous measure along the y -axis and the sin-
gular Cantorian measure along the x -axis.¹⁶ The latter is con-
structed as the weak limit of a sequence of measures which
give equal weight 2^{-n} to the 2^n closed intervals of length 3^{-n}
which contain the Cantor set for all n . The Fourier transform
of this measure, say, μ_x , is known.¹⁷ If we consider the ob-
servable x , the characteristic function of the asymptotic error
will be $\int e^{ixu} d\mu_x \int e^{ixu} d\mu_\varepsilon$. Let us suppose that the stationary
measure is close to the SRB measure, which is the case since
the Baker's transformation is uniformly hyperbolic, belongs
to the class \mathcal{M} , and is stochastically stable. Therefore for
small ε we could assume that the second integral in the pre-
ceding product is taken with respect to μ_x , and thus our
characteristic function is $\varphi_\infty(u) = |\int e^{ixu} d\mu_x|^2$. The latter can
be computed: Zygmund¹⁷ gives (see also Ref. 18 for a
former study of this quantity) 616
617
618
619
620
621
622
623
624
625
626
627
628
629
630
631
632

$$\varphi_\infty(u) = \prod_{k=1}^{\infty} \cos^2[u3^{-k}]. \quad (28) \quad 633$$

Zygmund also proved that $\varphi_\infty(u)$ is not summable and we
recall that this is a sufficient condition in order to get the
inversion formula (11). Despite this, we compute numeri-
cally the improper integral transform (11) and we get an
excellent agreement with the numerical issues (Fig. 12). We
outline that even if for any spatial discretization Δx we can
numerically compute, obtaining the same result, the distribu-
tion function ρ_ε^n with three different methods [Monte Carlo
sampling of errors falling in the interval $[x, x+\Delta x]$, inverse
Fourier transform of Eq. (2), and inverse Fourier transform
of Eq. (28)], we are not sure that the process converges in the
 $\Delta x \rightarrow 0$ limit, since the inverse Fourier transform could be ill
defined (see Appendix D and the analogous discussion in
Sec. IV C). Figure 11 shows clearly that at the numerically
accessible Δx values the process still has not converged. 634
635
636
637
638
639
640
641
642
643
644
645
646
647
648

C. Intermittent map 649

The intermittent map on the torus is defined as 650

$$T_\alpha x = \begin{cases} x + 2^\alpha x^{\alpha+1} \bmod 1 & \text{if } 0 \leq x < \frac{1}{2} \\ x - 2^\alpha (1-x)^{\alpha+1} \bmod 1 & \text{if } \frac{1}{2} \leq x < 1 \end{cases} \quad (29) \quad 651$$

with $0 < \alpha < 1$. It has been proved by several authors that the
decay of correlations follows a power law as $n^{1-1/\alpha}$.¹⁹⁻²¹ This 652
653

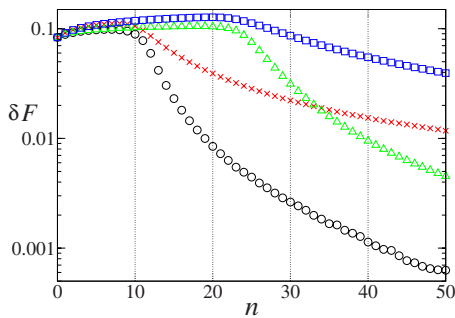


FIG. 13. (Color online) Decay of fidelity for the intermittent map, Monte Carlo integration with $N=10^7$. Black circles: $\varepsilon=10^{-4}$, $\alpha=0.5$. Red crosses: $\varepsilon=10^{-4}$, $\alpha=0.99$. Green triangles: $\varepsilon=10^{-8}$, $\alpha=0.5$. Blue squares: $\varepsilon=10^{-8}$, $\alpha=0.99$.

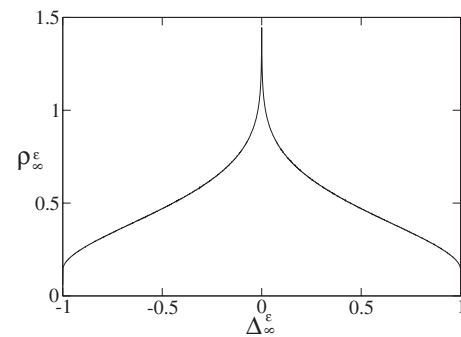


FIG. 14. ρ_∞^ε for the intermittent map, $\alpha=0.5$, $\varepsilon=10^{-8}$. Monte Carlo sampling using $N=10^9$ and $\Delta x=10^{-3}$.

654 rate is optimal in the sense that it gives also a lower bound
 655 for a large class of observables vanishing in a neighborhood
 656 of the neutral fixed point.^{22,23} The density h of the absolutely
 657 continuous invariant measure has a singularity in the neigh-
 658 borhood of zero of the type $x^{-\alpha}$. The density h_ε of the sta-
 659 tionary measure verifies the \mathcal{L}_m^1 estimate: $\|h-h_\varepsilon\|_{\mathcal{L}_m^1} \sim \varepsilon^{1-\alpha}$.²⁴
 660 It is interesting to remark that the problem of the stochastic
 661 stability for this map is not fully understood. The papers^{25,26}
 662 prove the weak convergence of the absolutely continuous
 663 stationary measure (under the additive noise) to a convex
 664 combination of the absolutely continuous invariant measure
 665 and of the Dirac mass at the neutral fixed point. The presence
 666 of this atomic measure in the weak limit is questionable; it
 667 prevents also any kind of strong convergence (in the \mathcal{L}_m^1
 668 sense).

669 Our Monte Carlo integrations for the decay of correla-
 670 tions are compatible with the analytically predicted power
 671 law, even if an exact computation of the exponent of the
 672 power law is not feasible to a numerical analysis since the
 673 convergence to the predicted law is slow in n . The decay of
 674 fidelity for this map shows a growing phase (that depends on
 675 α and is due to the convergence to the asymptotic measure),
 676 an α independent outset of decay $n_*(\varepsilon)$ (end of “plateau”)
 677 whose ε dependence is in qualitative agreement with Eq.
 678 (20), followed by an α , ε dependent decay law (Fig. 13). Our
 679 results show that in the $\varepsilon \rightarrow 0$ limit the decay law is compat-
 680 ible with a power law (the exponent seems to be higher than
 681 the one of the decay of correlations), while for high values of
 682 ε the decay law appears to be at least exponential. As a guess
 683 we claim a decay law $n^{-b}f(\varepsilon, n)$, where $f(\varepsilon, n)$ should be
 684 bounded by the decay law for translation and identity, Eq.
 685 (16). We checked that n_* corresponds to the beginning of the
 686 transition from the delta function to the asymptotic error dis-
 687 tribution function (not shown) and that Eq. (2) holds for ρ_∞^ε
 688 (which is shown in Fig. 14). We believe that the proposed
 689 decay law is also satisfied by the annealed random correla-
 690 tion integral given by the left-hand side of Eq. (6): this is a
 691 nice theoretical challenge.

692 Equation (D1) predicts a divergence for the asymptotic
 693 distribution ρ_∞^ε in 0 whenever $\alpha > 1/2$. We have indeed veri-
 694 fied that the height of $\rho_\infty^\varepsilon(0)$, numerically computed using a

Monte Carlo sampling with space discretization Δx , grows 695
 for the numerically accessible values of Δx , at least as 696
 $\log(\Delta x)$. 697

D. Quadratic map 698

We consider in this section the quadratic map $T_a x = a$ 699
 $-x^2$, $a > 0$. The image under T_a of $[-\sqrt{2a}, \sqrt{2a}]$ is $[-a, a]$ and 700
 thus for $a < 2$ we can define the perturbed map $T_{a,\varepsilon\eta} x = a$ 701
 $-x^2 + \varepsilon\eta$ from $[-\sqrt{2a}, \sqrt{2a}]$ to itself provided that $\varepsilon < \sqrt{2a} - a$. 702

This class of maps has been investigated in Ref. 27 from 703
 the point of view of stochastic stability. First of all the au- 704
 thors restricted the choice of the parameter a to the set of 705
 positive measure for which there exists a unique absolutely 706
 continuous invariant measure with density h (Jakobson’s 707
 theorem²⁸). For those values, the map satisfies also the 708
 Benedicks–Carleson¹⁴ conditions which were important for 709
 establishing the other perturbative results under the additive 710
 noise, namely, (i) the existence of an absolutely continuous 711
 stationary measure with density h_ε which converges in the 712
 \mathcal{L}_m^1 norm to h (stochastic stability) and (ii) the existence of 713
 exponential decay of correlations for the unperturbed map 714
 and for the perturbed system with decay rates which are uni- 715
 formly bounded in the noise (provided ε is small enough), as 716
 in formulas (5) and (6). The latter (see Ref. 9) allows us to 717
 apply Theorem 1 on the fidelity so that the estimate (12) for 718
 the rate of convergence to the characteristic function of the 719
 asymptotic error holds. We verified, through a bifurcation 720
 analysis, that in a neighborhood of $a=1.6$ the map is chaotic, 721
 and thus we have used this value for our investigation. 722

After a transient (which is due to the difference between 723
 the uniform distribution we use as initial condition for our 724
 Monte Carlo method and the invariant measure of the map) 725
 there is a plateau that ends at n_* , whose ε dependence is in 726
 qualitative agreement with Eq. (20), Fig. 15. To n_* corre- 727
 sponds the beginning of the transition of the error distribu- 728
 tion function (not shown). The asymptotic error distribution 729
 is shown in Fig. 16 [we have verified that the same result can 730
 also be obtained using Eq. (2)]. 731

E. Standard map 732

We study the standard map defined as 733

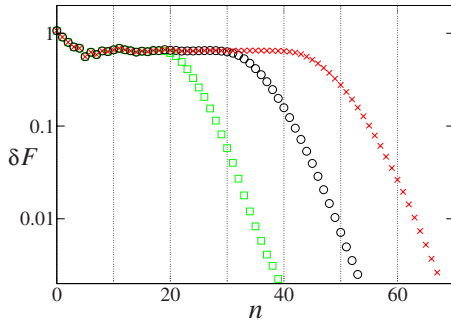


FIG. 15. (Color online) Decay of fidelity for the quadratic map, $a=1.6$, Monte Carlo integration with $N=10^8$. Green squares: $\varepsilon=10^{-4}$. Black circles: $\varepsilon=10^{-6}$. Red crosses: $\varepsilon=10^{-8}$.

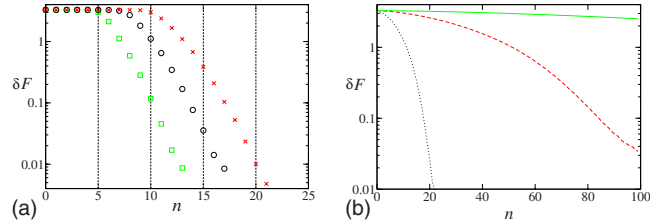


FIG. 17. (Color online) Decay of fidelity for the standard map, x observable, Monte Carlo integration with $N=10^7$. (a) $K=10$ (green squares: $\varepsilon=10^{-4}$; black circles: $\varepsilon=10^{-6}$; red crosses: $\varepsilon=10^{-8}$). (b) $K=10^{-2}$ (black, dotted: $\varepsilon=10^{-1}$; red, dashed: $\varepsilon=10^{-2}$; green: $\varepsilon=10^{-3}$).

734
$$T_{\mathbf{x}} = \begin{cases} y' = y + K \sin(x) \\ x' = x + y'. \end{cases} \quad (30)$$

735 We analyze its behavior considering three values of K : $K=10$
 736 (chaotic behavior), $K=10^{-2}$ (regular behavior), and $K=2$
 737 (mixed behavior). We recall that the breakup of the last in-
 738 variant curve corresponding to the golden mean frequency
 739 occurs for $K \approx 1$.

740 *Case $K=10$:* The chaotic case can be easily understood
 741 using the framework developed for other maps. For the de-
 742 cay of fidelity we have a plateau, followed by an outset of
 743 decay that occurs at n_* in qualitative agreement with Eq. (20)
 744 [(a) of Fig. 17]. n_* corresponds to the beginning of the tran-
 745 sient of the error function. The asymptotic error function ρ_∞^ε
 746 is triangular and Eq. (2) applies.

747 *Case $K=10^{-2}$:* In the regular regime there is no clear
 748 outset of decay, but just an ε dependent decay law [(b) of
 749 Fig. 17]. The asymptotic error function is reached when the
 750 fidelity reaches a value of a few orders of magnitude lower
 751 than its initial value. The asymptotic error function is trian-
 752 gular and Eq. (2) holds. The decay for y follows the same
 753 law as rotations on the circle, while the decay for x is
 754 quicker. This can be easily understood by considering the
 755 map where $K \sin(x)$ is replaced by $K\xi$, where ξ is a random
 756 variable in $[-1, 1]$. In the continuum limit $K \rightarrow 0$, see Appen-
 757 dix C, we have a diffusive process with Gaussian distribution
 758 where the mean square deviation is $K^2 n$ for the y variable,
 759 $K^2 n^3$ for the x variable proving that the relaxation for the
 760 latter is faster.

761 *Case $K=2$:* For $K=2$ the system exhibits features of both

regular and chaotic maps. The decay of fidelity presents a
 762 plateau ending at n_* in agreement with Eq. (20). This phase
 763 is followed by a quick, almost ε independent decay phase,
 764 and then by a slower ε dependent phase (Fig. 18). After the
 765 first quick decay phase we reach an asymptotic error function
 766 for the chaotic component only, while if ε is low enough, we
 767 still have a δ function for the regular component (Fig. 19).
 768 For low values of ε we can consider this as a “metastable
 769 error distribution function” since it does not change during a
 770 time scale much longer than the decay of the chaotic compo-
 771 nent. The study of the ε dependent decay phase of the
 772 regular component in a map with mixed behavior is more
 773 difficult than for a regular map, probably due to the interac-
 774 tion between the chaotic and regular components. Indeed, for
 775 purely chaotic and regular maps we found that the decay of
 776 fidelity was almost independent of the function ψ , and thus
 777 we limited ourselves to the study of the less computationally
 778 expensive $\psi(\mathbf{x})=x$. But for the standard map with $K=2$ even
 779 when the fidelity for $\psi(\mathbf{x})=x$ has reached a value of a few
 780 orders of magnitude lower than its initial value, the error
 781 function has not reached its asymptotic value (triangular dis-
 782 tribution). Since the error distribution ρ_ε^n is given by the Fou-
 783 rier transform of $\varphi_\varepsilon^n(u)$, i.e., by the fidelity computed using
 784 $\psi_1 = \psi_2 = e^{iu x}$, the time scales of the transient of ρ_ε^n are deter-
 785 mined by the decay of fidelity of $e^{iu x}$. While for all the pre-
 786 viously studied systems the decay of fidelity for $e^{iu x}$ resulted
 787 to be u independent, and thus the system had a single decay
 788 time scale, for the standard map with $K=2$ the decay of $e^{iu x}$
 789 results to be strongly u dependent (see Fig. 20; the change in
 790 slope around $n \approx 50$ corresponds to the end of the decay of
 791 the chaotic component and the beginning of the “metastable”
 792 phase, which is quite short for $\varepsilon=10^{-1}$ but considerably
 793

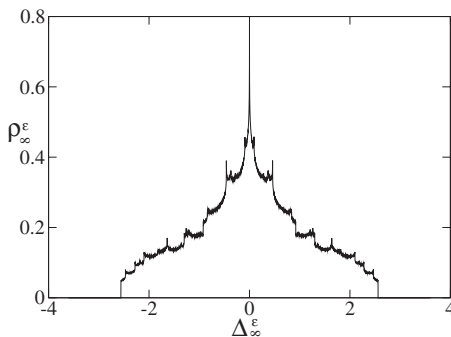


FIG. 16. ρ_∞^ε for the quadratic map, $a=1.6$, $\varepsilon=10^{-8}$. Monte Carlo sampling using $N=10^9$ and $\Delta x=10^{-3}$.

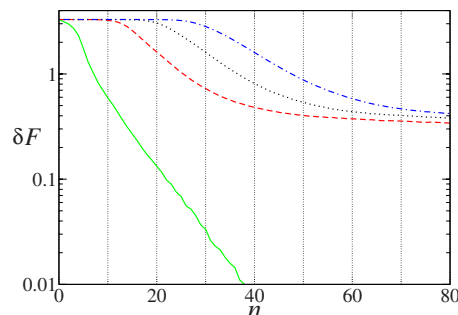


FIG. 18. (Color online) Decay of fidelity for the standard map, x observable, $K=2$, Monte Carlo integration with $N=10^7$. Green: $\varepsilon=10^{-4}$. Red, dashed: $\varepsilon=10^{-4}$. Black, dotted: $\varepsilon=10^{-6}$. Blue, dot-dashed: $\varepsilon=10^{-8}$.

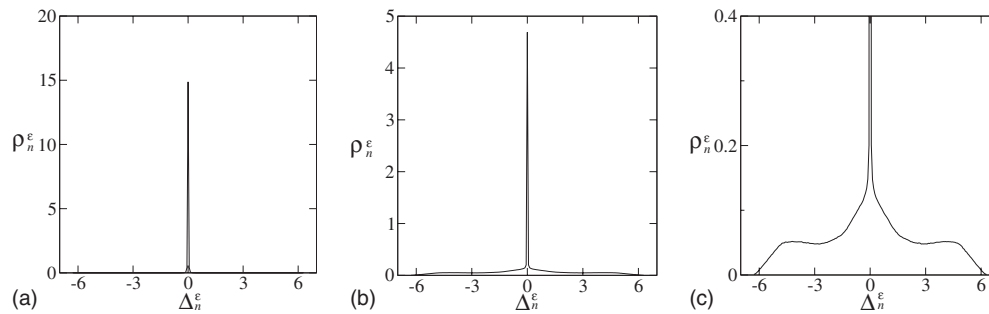


FIG. 19. ρ_n^ε for the standard map, $K=2$, $\varepsilon=10^{-4}$, x observable. (a) $n=9$; (b) $n=49$; (c) detail of the metastable distribution (ρ_{49}). Monte Carlo sampling using $N=10^7$ and $\Delta x=\pi/50$.

794 longer for lower values of ε), and thus the regular component
 795 of a map with mixed behavior has not a single decay scale.
 796 We have verified that when the fidelity computed using e^{ix} ,
 797 which, on the basis of our numerical tests, has probably the
 798 longest decay time, reaches a value of $\approx 10^{-3}$, we have the
 799 convergence to the triangular asymptotic error distribution
 800 ρ_∞^ε .

801 V. CONCLUSIONS

802 We have analyzed the statistical properties of the error
 803 introduced by an additive random noise in a discrete dynamical
 804 system by comparing the distributions obtained from
 805 Monte Carlo computations and from the fidelity, which, for a
 806 suitable choice of the observables, provides the Fourier
 807 transform of the pdf of the error. This pdf is obtained in the
 808 limit of large iteration time and the rate of this convergence
 809 is very important to discriminate between regular and chaotic
 810 motions. For rotations and Bernoulli maps an exact result
 811 and an optimal estimate for the convergence rate are ob-
 812 tained. The exponential convergence rate for regular maps
 813 and the superexponential one for chaotic maps appear to be
 814 quite general as we indicate by several numerical examples.
 815 The initial distribution of errors is a Dirac δ function with
 816 support at zero, whereas the asymptotic distribution depends
 817 on the invariant and the stationary measures. When both are
 818 Lebesgue the asymptotic distribution is triangular as for two
 819 points randomly chosen on an interval. For measures abso-
 820 lutely continuous with respect to Lebesgue the asymptotic
 821 distribution is smooth, whereas it is spiky for singular con-
 822 tinuous measures typical of attractors with a Cantorian struc-

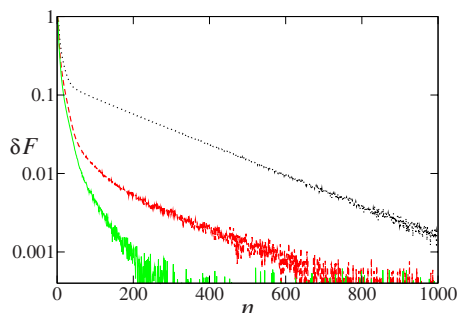


FIG. 20. (Color online) Decay of fidelity for the standard map, $K=2$, $\varepsilon=10^{-1}$, Monte Carlo integration with $N=10^7$. Black, dotted: $\psi_1=\psi_2^*=e^{ix}$. Red, dashed: $\psi_1=\psi_2^*=e^{i2x}$. Green: $\psi_1=\psi_2^*=e^{i3x}$.

ture (fractals). As we said above, the ergodic properties of
 the map are reflected in the way the asymptotic limit is
 reached: the exponential and superexponential convergence
 rates are the same as for a random walk when the determin-
 istic evolution is linear or exponential as it can be easily
 proved in the continuum limit. Whereas the asymptotic limit
 is reached smoothly for regular maps, for the chaotic ones
 there is a sharp transition whose location depends only on
 the perturbation strength. For maps with chaotic and regular
 invariant regions, such as the standard map short after the
 breakup of the last invariant curve, there is first a sharp tran-
 sition followed by a smooth decay. Finally the procedure we
 outlined applies to the analysis of roundoff errors for the
 numerical maps, a key issue in the numerical analysis of
 dynamical systems. We have already applied the procedure
 developed in this paper to analyze the roundoff errors and the
 results will be soon submitted for publication. We can antici-
 pate that the global error grows linearly for regular maps and
 exponentially for chaotic maps, while the asymptotic error
 distribution reflects the properties of the invariant measure.
 The convergence rate of fidelity can be quite different from
 the one observed for additive noise due to the deterministic
 nature of roundoff, nevertheless by increasing the complexity
 of the map the “pseudorandom” character of roundoff errors
 becomes more pronounced, and the decay law becomes, in
 particular for chaotic maps, equivalent to that of maps per-
 turbed with additive noise. To conclude we claim that we
 have provided a reliable and constructive tool to investigate
 analytically and numerically the perturbations induced by
 random errors. This procedure can be applied also to numeri-
 cal roundoff errors even though in that case no rigorous gen-
 eral results can be formulated because the algorithms imple-
 mented in finite precision arithmetic are hardware dependent.

ACKNOWLEDGMENTS

F.Z. has been partially supported by the GDRE 224
 GREFI-MEFI (jointly sponsored by the French CNRS and
 the Italian INDAM). The authors thank the anonymous ref-
 erees whose remarks and suggestions contributed to improve
 the paper.

862 APPENDIX A: COMPARISON TO SOME RESULTS 863 BY SAUER

864 We now compare our results with the work of Sauer in
865 Ref. 13. He considered a smooth observable g on the phase
866 space X and the algebraic difference

$$867 \quad \Delta(g) \equiv \langle g \rangle_{\text{computed}} - \langle g \rangle_{\text{true}},$$

868 where $\langle g \rangle_{\text{true}}$ is the ergodic average computed along the true
869 trajectory of T and $\langle g \rangle_{\text{computed}}$ is the ergodic average com-
870 puted along the perturbed orbit with noise size ε . Sauer pro-
871 posed the following heuristic scaling:

$$872 \quad \Delta(g) = K\varepsilon^h,$$

873 where K is a constant and h is an “exponent expressing the
874 severity of the fluctuations of the Lyapunov exponent.”¹³

875 For a map belonging to the class \mathcal{M} , we simply have
876 $\langle g \rangle_{\text{true}} = \int_X g d\mu$. The ergodic average for the random pertur-
877 bations introduced in Sec. II C will be

$$878 \quad \lim_{n \rightarrow \infty} \frac{1}{n} \sum_{l=0}^{n-1} g(T_{\omega_l} T_{\omega_{l-1}} \cdots T_{\omega_0} x).$$

879 For the maps in \mathcal{M} the stationary measure is ergodic and this
880 means that the previous Birkhoff sum goes to $\int_X g d\mu_\varepsilon$, for x
881 chosen m —almost everywhere and for almost all the realiza-
882 tions ω taken with respect to the measure θ_ε^N ; see, for in-
883 stance, Ref. 29. It is therefore reasonable to put $\langle g \rangle_{\text{computed}}$
884 $= \int_X g d\mu_\varepsilon$ in such a way that

$$885 \quad \Delta(g) = \int_X g d\mu_\varepsilon - \int_X g d\mu$$

886 [compare with (i) in Remark 2]. Now, let us suppose that the
887 map $T \in \mathcal{M}$ has an invariant measure μ which is absolutely
888 continuous with respect to the Lebesgue measure m with
889 density h ; we suppose also that the stationary measure μ_ε is
890 absolutely continuous with density h_ε . The systems in \mathcal{M}
891 usually enjoy the *strong* stochastic stability property which
892 means the convergence of h_ε to h in the \mathcal{L}_m^1 norm. The
893 paper²⁴ quotes several examples where this \mathcal{L}_m^1 convergence
894 is explicitly computed for additive noise, with rigorous argu-
895 ments or numerically (even for systems outside \mathcal{M}), as a
896 function of the noise size ε ; the scalings found are of the
897 type

$$898 \quad \|h - h_\varepsilon\|_{\mathcal{L}_m^1} \leq \text{const } \varepsilon^\gamma, \quad (\text{A1})$$

899 where γ is an exponent depending upon the map T . This
900 exponent seems related to the smoothness of the map rather
901 than to the Lyapunov exponent. For example, for continuous
902 uniformly expanding maps of the circle $\gamma=2$, while $\gamma=1$ if
903 the map has discontinuities and it is therefore piecewise ex-
904 panding. For Misiurewicz quadratic maps (see also Sec.
905 IV D), $\gamma=0.5$ and it ranges between 0.3 and 0.7 for the in-
906 termittent map investigated in Sect. IV C. We have also seen
907 that there are examples for which the invariant and the sta-
908 tionary measure are the same, $h=h_\varepsilon$, but the pdf of the
909 asymptotic error for the observable identity $f(x)=x$ is a
910 smooth function whose support has diameter twice the sup-
911 port of the invariant measure.

Since, by Hölder inequality,

$$|\Delta(g)| \leq \|g\|_{C^0} \|h - h_\varepsilon\|_{\mathcal{L}_m^1} \|g\|_{C^0} \text{const } \varepsilon^\gamma, \quad 913$$

the comparison with the previous bound claimed by Sauer is
not obvious especially for the meaning of the scaling expo-
nent of ε . One possible explanation, which deserves better
investigation, is that the fluctuations of the Lyapunov expo-
nent play a role whenever we replace $\langle g \rangle_{\text{computed}}$ with the
Birkhoff sum $1/n \sum_{l=0}^{n-1} g(T_{\omega_l} T_{\omega_{l-1}} \cdots T_{\omega_0}(x))$ for finite n and
we take into account the limits for small ε and large n .

Another explanation is that Sauer’s result holds for dif-
feomorphisms admitting a SRB measure which is singular
with respect to Lebesgue and with more than one Lyapunov
exponent. In this case we lose the comparison of the densi-
ties given by Eq. (A1) and we should evaluate directly the
difference $\int_X g d\mu_\varepsilon - \int_X g d\mu$: this is done, for example, for
uniformly hyperbolic attractors in Ref. 30 and for the Hénon
attractor in Ref. 15, but there is no explicit scaling in ε .

APPENDIX B: COMPUTATION OF FIDELITY FOR $qx \bmod 1$

The iterated perturbed map is defined as

$$T_\varepsilon^n = q^n x + \varepsilon(q^{n-1} \xi_1 + q^{n-2} \xi_2 + \cdots + q \xi_{n-1} + \xi_n) \bmod 1. \quad 932$$

The fidelity for functions ϕ, ψ which are piecewise C^1 with
a finite number of discontinuities is given by

$$933 \quad F_n^\varepsilon = \sum_{k,k'} \phi_k \psi_{k'} \int_0^1 e^{2\pi i q^n (k-k')x} dx \int_{-1}^1 \frac{d\xi}{2^n} e^{2\pi i k' \varepsilon (q^{n-1} \xi_1 + \cdots + \xi_n)} \quad 935$$

$$= \phi_0 \psi_0 + \sum_{|k| \geq 1} \phi_k \psi_{-k} S_{n,q}(k\varepsilon). \quad (\text{B1}) \quad 936$$

It is trivial to check that the decay of fidelity for any trans-
lation on the torus is equivalent to that of the identity $Tx=x$,
and thus since $S_{n,q}(x) \equiv S^n(x)$, Eq. (B1) implies both Eqs.
(14) and (17).

To estimate $S_{n,q}(x)$ we can use the bound (15) for $S(x)$,
but we have to distinguish between three regions (we assume
 $x>0$, in the general case substitute x with $|x|$): region 1,
where $q^{n-1}x < 1$, in which we can use, setting $\alpha = \log(2\pi)$

$$|S_{n,q}(x)| \leq e^{-\alpha x^2(1+q^2+\cdots+q^{2(n-1)})} \leq e^{-\alpha x^2 q^{2(n-1)}}, \quad 945$$

region 3 where

$$xqx \cdots q^{n-1}x = x^n q^{1+2+\cdots+n-1} = (xq^{(n-1)/2})^n > 1 \quad 947$$

or, equivalently, $xq^{(n-1)/2} > 1$, and thus we can use

$$|S_{n,q}(x)| \leq (2\pi x q^{(n-1)/2})^{-n}, \quad 949$$

and an intermediate region 2 where $xq^{-(n-1)/2} < 1 < xq^n$. To
analyze the behavior of the function in the latter region let us
assume that $xq^{m-1} < 1 < xq^m$ with integer $(n-1)/2 < m < n$.
We can estimate in a different way the terms with xq^l greater
or smaller than 1, and thus

$$\begin{aligned}
 |S_{n,q}(x)| &\leq \frac{(2\pi)^{-(n-m)}}{xq^m xq^{m-1} \dots xq^{n-1}} e^{-\alpha x^2(1+q^2+\dots+q^{2(m-1)})} \\
 &\leq (2\pi xq^{(n+m-1)/2})^{-(n-m)} e^{-\alpha x^2 q^{2(m-1)}} \\
 &\leq (2\pi q^{(n-m-1)/2})^{-(n-m)} e^{-\alpha x^2 q^{2(m-1)}}.
 \end{aligned}$$

We can thus use the following bound for $S_{n,q}(x)$:

$$|S_{n,q}(x)| \leq \begin{cases} \exp(-\alpha x^2 q^{2(n-1)}) & \text{if } xq^{n-1} < 1 \\ (2\pi q^{(n-m-1)/2})^{-(n-m)} e^{-\alpha x^2 q^{2(m-1)}} & \text{if } xq^{m-1} < 1 < xq^m \text{ with } (n-1)/2 < m < n \\ (2\pi xq^{(n-1)/2})^{-n} & \text{if } xq^{(n-1)/2} > 1, \end{cases}$$

where we have once again $\alpha = \log(2\pi)$. [When $q=1$ there is no region 2, and in region 1 the more accurate bound $S^n(x) \leq e^{-\alpha x^2 n}$ can be used.]

Using the estimates on $S_{n,q}(x)$ we provide bounds to the fidelity in three different regions. It is convenient to introduce an integer n_* defined by $n_* = \{-\log_q \varepsilon\}$, where $\{x\}$ denotes the integer closest to the real x , so that

$$\varepsilon \approx q^{-n_*}.$$

Region I: $\varepsilon q^{n-1} < 1$. Using the Fourier expansion for the fidelity (B1) we write

$$|F_n - \phi_0 \psi_0| \leq \sum_{k \neq 0} |\phi_k \psi_{-k}| |S_{n,q}(k\varepsilon)| = R_1 + R_2 + R_3,$$

where the term R_1 corresponds to the contribution of all the Fourier components with $|k|\varepsilon q^{n-1} < 1$, the term R_2 to the components with $|k|\varepsilon q^{(n-1)/2} < 1 < |k|\varepsilon q^{n-1}$, and the term R_3 to the components with $|k|\varepsilon q^{(n-1)/2} > 1$.

The following bound holds for the first term R_1 ,

$$\begin{aligned}
 R_1 &\leq \sum_{|k|=1}^{(\varepsilon q^{n-1})^{-1}} |\phi_k \psi_{-k}| e^{-\alpha \varepsilon^2 k^2 q^{2(n-1)}} \\
 &\leq e^{-\alpha \varepsilon^2 q^{2(n-1)}} 2 \sum_{k=1}^{(\varepsilon q^{n-1})^{-1}} \frac{1}{k^2} \leq 2(2 - \varepsilon q^{n-1}) e^{-\alpha \varepsilon^2 q^{2(n-1)}},
 \end{aligned}$$

where we have assumed once again that the Fourier coefficients decay as $|k|^{-1}$ and we have used the following estimate:

$$\sum_{k=A}^B \frac{1}{k^2} \leq \frac{1}{A^2} + \int_A^B \frac{dk}{k^2} = \frac{1}{A^2} + \frac{1}{A} - \frac{1}{B} \leq \frac{2}{A} - \frac{1}{B}$$

for $B > A \geq 1$. The second term R_2 has the following bound:

$$\begin{aligned}
 R_2 &\leq \sum_{m=(n+1)/2}^{n-1} (2\pi q^{(n-m-1)/2})^{-(n-m)} \sum_{|k|=(\varepsilon q^m)^{-1}}^{|k|=(\varepsilon q^{m-1})^{-1}} \frac{e^{-\alpha k^2 \varepsilon^2 q^{2(m-1)}}}{k^2} \\
 &\leq \sum_{m=(n+1)/2}^{n-1} (2\pi q^{(n-m-1)/2})^{-(n-m)} e^{-\alpha \varepsilon^2 q^2} 2\varepsilon q^m (2 - q^{-1}) \\
 &\leq \frac{e^{-\alpha \varepsilon^2 q^2}}{2\pi} 2\varepsilon \left(2 - \frac{1}{q}\right) \sum_{m=n+1/2}^{n-1} q^m \\
 &\leq 4\varepsilon q^n \frac{e^{-\alpha \varepsilon^2 q^2}}{2\pi(q-1)} \leq 2\varepsilon q^{n-1}.
 \end{aligned}$$

For the third term R_3 we have the bound

$$\begin{aligned}
 R_3 &\leq \sum_{|k| \geq (\varepsilon q^{(n-1)/2})^{-1}}^{\infty} \frac{1}{k^2} \frac{1}{(2\pi \varepsilon |k| q^{(n-1)/2})^n} \\
 &\leq \frac{2}{(2\pi \varepsilon q^{(n-1)/2})^n} \left((\varepsilon q^{(n-1)/2})^{n+2} + \int_{(\varepsilon q^{(n-1)/2})^{-1}}^{\infty} \frac{dk}{k^{n+2}} \right) \\
 &= \frac{2}{(2\pi)^n} \varepsilon q^{(n-1)/2} \left(\frac{1}{n+1} + \varepsilon q^{(n-1)/2} \right) \\
 &\leq \frac{4}{(2\pi)^n} \varepsilon q^{(n-1)/2}.
 \end{aligned}$$

Finally the estimate in this region reads

$$\begin{aligned}
 |F_n - \phi_0 \psi_0| &\leq 2(2 - \varepsilon q^{n-1}) e^{-\alpha \varepsilon^2 q^{2(n-1)}} + 2\varepsilon q^{n-1} \\
 &\quad + \frac{4}{(2\pi)^n} \varepsilon q^{(n-1)/2},
 \end{aligned} \tag{B2}$$

which for $q=1$ leads to Eq. (16).

- Region II: $\varepsilon q^{(n-1)/2} < 1 < \varepsilon q^{n-1}$. In this region the estimate is not very accurate. First of all R_1 vanishes since the upper limit in the sum, namely, $(\varepsilon q^{n-1})^{-1}$, is smaller than the lower limit. The second term R_2 , which is evaluated above for $\varepsilon q^{n-1} \approx 1$, is of order 1, whereas the last term R_3 is small with respect to 1.
- Region III: $\varepsilon q^{(n-1)/2} > 1$. In this region the contributions of R_1 and R_2 vanish and we are left just with R_3 which reads

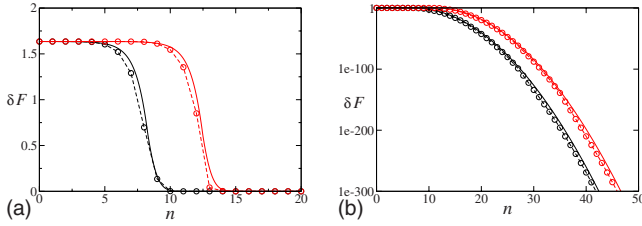


FIG. 21. (Color online) Comparison between the analytical result (B1) (dashed lines and circles) and the estimate (B5) (continuous lines) using $\phi_k = \psi_k = k^{-1}$ truncated at $k=100$. Black: $\varepsilon=10^{-4}$. Red (gray in black and white): $\varepsilon=10^{-6}$ [(b) logarithmic plot].

$$\begin{aligned}
 1008 \quad R_3 &\leq \sum_{|k|=1}^{\infty} \frac{1}{k^2} \frac{1}{(2\pi\varepsilon|k|q^{(n-1)/2})^n} \\
 1009 \quad &= 2 \left(1 + \int_1^{\infty} \frac{dk}{k^{n+2}} \right) \frac{1}{(2\pi\varepsilon q^{(n-1)/2})^n} \\
 1010 \quad &= \frac{n+2}{n+1} \frac{2}{(2\pi\varepsilon q^{(n-1)/2})^n}. \quad (B3)
 \end{aligned}$$

1011 1. Fit and comparison to Monte Carlo 1012 simulations

1013 The validity of the previous estimates has been checked
1014 with numerical calculations. We first write Eq. (B3) using
1015 $\varepsilon = q^{-n_*}$ so that

$$1016 \quad R_3 \leq 3 \left(\frac{q^{1/2}}{2\pi} \right)^n q^{n_*} q^{-n^2/2} = 3q^{n_*^2/2} \left(\frac{q^{1/2}}{2\pi} \right)^n q^{-(n-n_*)^2/2},$$

1017 valid for $\varepsilon q^{(n-1)/2} > 1$. From the estimate (B2) and the present
1018 one we finally obtain

$$|F_n - \phi_0 \psi_0| \leq \begin{cases} 2(2 - \varepsilon q^{n-1}) e^{-\alpha \varepsilon^2 q^{2(n-1)}} + 2\varepsilon q^{n-1} & \text{if } n < n_* + 1 \\ 3q^{n_*^2/2} \left(\frac{q^{1/2}}{2\pi} \right)^n q^{-(n-n_*)^2/2} & \text{if } n \geq 2n_* + 1. \end{cases} \quad (B4)$$

1020 We can fit the fidelity with a formula derived from the pre-
1021 vious estimates by extending the estimate in region III to
1022 region II according to

$$1023 \quad |F_n - \phi_0 \psi_0| \simeq \begin{cases} A e^{-\alpha q^{2(n-n_*)}} & \text{if } n \leq n_* \\ A e^{-\alpha'} q^{-(n-n_*)^2/2} & \text{if } n > n_*, \end{cases} \quad (B5)$$

1024 where A is a constant of order 1. We can evaluate the width
1025 of the transition Δn requiring that at $n = n_* - \Delta n$ the decay of
1026 fidelity $\delta F_n = |F_n - \phi_0 \psi_0|$ assumes a value some percent below
1027 A [at $n = n_*$ its value is $A e^{-\alpha} = A(2\pi)^{-1} = 0.16A$]. Choosing,
1028 for instance, $\delta F_{n_* - \Delta n} = A e^{\alpha e^{-4}} \simeq 0.97A$ we find

$$1029 \quad \Delta n = \frac{2}{\log q}.$$

1030 The validity of the analytical result (B1) has been checked
1031 with a Monte Carlo simulation (Fig. 1). We found (Fig. 21)

that the analytical result (B1) can be fitted very well by
Eq. (B5).

We outline that due to the extremely quick decay of the
 $e^{-\alpha \varepsilon^2 q^{2(n-1)}}$ term around n_* , the fit (B5) can be sketched as a
plateau of length $n_*(\varepsilon)$ followed by an ε independent decay
law.

APPENDIX C: THE CONTINUUM LIMIT

A map on the torus \mathbb{T} with a random perturbation

$$x_{n+1} = x_n + \Delta t \phi(x_n) + \varepsilon \sqrt{\Delta t} \xi_n,$$

where ξ_n are random variables with zero average and unit
variance, becomes in the limit $\Delta t \rightarrow 0$ the Langevin equation

$$\dot{x} = \phi(x) + \varepsilon \xi(t),$$

setting $\xi(t)dt = dw(t)$ where $w(t)$ is a Wiener process and $\xi(t)$
a distribution known as white noise. The probability density
distribution $\rho(x, t)$ satisfies the Fokker-Planck equation

$$\frac{\partial \rho}{\partial t} + \phi(x)\rho = \frac{\varepsilon^2}{2} \frac{\partial^2 \rho}{\partial x^2}$$

with boundary conditions $\rho(0, t) = \rho(1, t)$ and initial condition
 $\rho(x, 0) = \rho_0(x)$. The fundamental solution $G(x, t; x_0, 0)$ satis-
fies the same equation with initial condition $G(x, 0; x_0, 0)$
 $= \delta(x - x_0)$. As a consequence, we have

$$\rho(x, t) = \int_0^1 dx_0 G(x, t; x_0, 0) \rho_0(x_0).$$

Letting $G_{\mathbb{R}}$ be the fundamental solution defined in \mathbb{R} the
corresponding solution for the torus \mathbb{T} is given by

$$G_{\varepsilon}(x, t; x_0, t) = \sum_{n=-\infty}^{+\infty} G_{\mathbb{R}}(x + n, t; x_0, 0) = \sum_{k=-\infty}^{+\infty} C_k(t) e^{2\pi i k x}.$$

Simple calculations show that for $\phi(x) = \Omega$ and $\phi(x) = Ax$ the
Fourier coefficients are given by

$$C_k(t) = e^{-2\pi i k(x_0 + \Omega t)} e^{-2\pi^2 k^2 \varepsilon^2 t} \quad \text{if } \phi = \Omega,$$

$$C_k(t) = e^{-2\pi i k x_0 e^{At}} e^{-2\pi^2 k^2 \varepsilon^2 (e^{2At} - 1)/2A} \quad \text{if } \phi = Ax.$$

We notice that the unperturbed $\varepsilon=0$ fundamental solution is
 $G_0(x, t; x_0, t) = \delta(x - S_t(x_0))$, where $S_t(x_0) = x_0 + \Omega t$ if $\phi = \Omega$ and
 $S_t(x_0) = x_0 e^{At}$ if $\phi = Ax$.

Given two smooth observables $f(x)$, $g(x)$ the correla-
tions and the fidelity are defined by

$$C(t) = \int_0^1 dx_0 f(x_0) \int_0^1 dx G(x, t; x_0, 0) g(x),$$

$$F(t) = \int_0^1 dx_0 f(S_t(x_0)) \int_0^1 dx G(x, t; x_0, 0) g(x).$$

After the Fourier expansion of f and g and denoting with

$$1068 \quad F(t) = \sum_{k=-\infty}^{+\infty} \sum_{k'=-\infty}^{+\infty} f_{-k} e^{-2\pi^2 k'^2 \sigma^2(t)} g_{k'} \int_0^1 dx_0 e^{-2\pi i S_t(x_0)(k-k')},$$

1069 the mean square deviation of the stochastic processes satisfying $\dot{\eta} = \Omega + \epsilon \xi$ is $\sigma^2(t) = \epsilon^2 t$, whereas for $\dot{\eta} = Ax + \epsilon \xi$ it is given by $\sigma^2(t) = \epsilon^2 (e^{2At} - 1) / 2A$. The last integral is $\delta_{k',k}$ if $1072 S_t(x_0) = x_0 + \Omega t$ and $e^{i\theta} \theta^{-1} \sin \theta$ with $\theta = \pi e^{At}(k' - k)$, which 1073 approaches $\delta_{k',k}$ as $t > 0$ grows. As a consequence we may 1074 compare the results with the translations on the torus and the 1075 map $qx \bmod 1$ by setting $\omega = \Omega \Delta t$, $q = 1 + A \Delta t$, and $\epsilon_{\text{map}} = \epsilon \sqrt{\Delta t}$. Agreement is found with the fidelity for the maps if 1077 we let $\Delta t \rightarrow 0$ and $n \rightarrow \infty$ so that $n \Delta t = t$ finite.

1078 APPENDIX D: LÉVY'S INVERSION FORMULA

1079 Let us consider a 1D map on the unit interval $[0,1]$ and 1080 the observable identity $f(x) = x$. Suppose, moreover, that μ 1081 and μ_ϵ have absolutely continuous invariant densities h and 1082 h_ϵ , respectively, which are \mathcal{L}_m^1 very close in such a way that 1083 φ_∞^ϵ is approximately given by $\varphi_\infty^\epsilon(u) = |\int_{[0,1]} e^{iux} h(x) dx|^2$. Standard results on Fourier series immediately imply that φ_∞^ϵ is 1085 uniformly continuous on \mathbb{R} , bounded and vanishing at infinity (Riemann–Lebesgue). We now consider the interesting 1087 cases given by the intermittent maps of Sec. IV C and the 1088 quadratic maps of Sec. IV D for which the invariant density 1089 behaves like $h(x) \sim x^{-\alpha}$, with $0 < \alpha < 1$ for the intermittent 1090 maps and $\alpha = 0.5$ for the particular quadratic map with $a = 2$, 1091 and whenever x is close to 0 (for the quadratic map a change 1092 in variable brings the singularity from ± 1 to zero). We have, 1093 therefore, to investigate the asymptotic behavior for large $|u|$ 1094 of the integral

$$1095 \quad \varphi_\infty^\epsilon(u) = \left| \int_{[0,1]} \frac{e^{iux} r(x)}{x^\alpha} dx \right|^2, \quad 0 < \alpha < 1,$$

1096 where r is a bounded smooth function in the interval $[0,1]$. 1097 Now we have (Ref. 31, p. 519)

$$1098 \quad \left| \int_{[0,1]} \frac{e^{iux} r(x)}{x^\alpha} dx \right| = \mathcal{O}(|u|^{\alpha-1}), \quad |u| \text{ large.} \quad (D1)$$

1099 We could therefore conclude that whenever $\alpha < 1/2$ the characteristic function φ_∞^ϵ is summable and we can apply the 1100 Lévy inversion formula to get the density of the distribution 1101 function of the asymptotic error. Instead when $1/2 \leq \alpha < 1$ 1102 we should use a generalization of Eq. (11); if we call Φ_∞^ϵ the 1103 distribution function of Δ_∞^ϵ and if $-\infty < a < b < \infty$ are continuity points for Φ_∞^ϵ , then (Ref. 12, p. 264)

$$1106 \quad \Phi_\infty^\epsilon(b) - \Phi_\infty^\epsilon(a) = \lim_{C \rightarrow \infty} \frac{1}{2\pi} \int_{-C}^C \frac{e^{-ita} - e^{-itb}}{it} \varphi_\infty^\epsilon(t) dt.$$

1107 The integral on the right-hand side of the preceding formula 1108 is of course convergent for $0 < \alpha < 1$ and whenever $|C|$ goes 1109 to infinity. We have nevertheless proceeded to the numerical

computation of the improper integral $\rho_\infty^\epsilon(t)$ 1110 $= (2\pi)^{-1} \int_{-\infty}^{\infty} e^{-iut} \varphi_\infty^\epsilon(u) du \sim (2\pi)^{-1} \int_{-\infty}^{\infty} e^{-iut} / (u^{2-2\alpha}) du$, where 1111 $2-2\alpha \leq 1$ for $1/2 \leq \alpha$. We choose for simplicity $2-2\alpha < 1$, 1112 since the integrand $u^{2\alpha-2}$ is the asymptotic approximation, 1113 for large $|u|$, of the characteristic function $\varphi_\infty^\epsilon(u)$, and this one 1114 is surely integrable in the neighborhood of zero. It is well 1115 known that the Fourier transform of $u^{2\alpha-2}$ and for $2-2\alpha$ 1116 < 1 is of order $t^{1-2\alpha}$ in the *distribution* sense.³² Therefore the 1117 density $\rho_\infty^\epsilon(t)$ computed numerically blows up to infinity for t 1118 close to zero and we observed this fact for the intermittent 1119 and the quadratic map described above. We believe the same 1120 happens for the singular measure of the Baker map, but we 1121 do not even have a heuristic handling for this. 1122

¹D. Knuth, *The Art of Computer Programming* (Addison-Wesley, Reading, 1969), Vol. 2. 1123

²A. Katok and B. Hasselblatt, *Introduction to the Modern Theory of Dynamical Systems* (Cambridge University Press, Cambridge, 1995). 1125

³S. M. Hammel, J. A. Yorke, and C. Grebogi, *J. Complex.* **3**, 136 (1987). 1127

⁴S. M. Hammel, J. A. Yorke, and C. Grebogi, *Bull. Am. Math. Soc.* **19**, 465 (1988). 1128

⁵C. Grebogi, S. Hammel, J. Yorke, and T. Sauer, *Phys. Rev. Lett.* **65**, 1527 (1990). 1130

⁶S. N. Chow and K. Palmer, *J. Dyn. Differ. Equ.* **3**, 361 (1991). 1132

⁷E. S. Van Vleck, *SIAM J. Sci. Comput. (USA)* **16**, 1177 (1995). 1133

⁸T. Sauer, C. Grebogi, and J. Yorke, *Phys. Rev. Lett.* **79**, 59 (1997). 1134

⁹C. Liverani, Ph. Marie, and S. Vaienti, *J. Stat. Phys.* **128**, 1079 (2007). 1135

¹⁰G. Benenti, G. Casati, and G. Velbe, *Phys. Rev. E* **67**, 055202 (2003). 1136

¹¹H. Hu, Ph. Marie, and S. Vaienti (unpublished). 1137

¹²Y. S. Chow and H. Teicher, *Probability Theory* (Springer-Verlag, Berlin, 1978). 1138

¹³T. Sauer, *Phys. Rev. E* **65**, 036220 (2002). 1140

¹⁴M. Benedicks and L. Carleson, *Ann. Math.* **133**, 73 (1991). 1141

¹⁵M. Benedicks and M. Viana, *Ann. Inst. Henri Poincaré, Anal. Non Linéaire* **23**, 713 (2006). 1142

¹⁶D. Bessis, G. Paladin, G. Turchetti, and S. Vaienti, *J. Stat. Phys.* **51**, 109 (1988). 1145

¹⁷A. Zygmund, *Trigonometrical Series*, 2nd ed. (Cambridge University Press, Cambridge, 1968). 1146

¹⁸D. Bessis, J. D. Fournier, G. Servizi, and G. Turchetti, *Phys. Rev. A* **36**, 920 (1987). 1148

¹⁹C. Liverani, B. Saussol, and S. Vaienti, *Ergod. Theory Dyn. Syst.* **19**, 671 (1999). 1150

²⁰L. S. Young, *Isr. J. Math.* **110**, 153 (1999). 1152

²¹H. Hu, *Ergod. Theory Dyn. Syst.* **24**, 495 (2004). 1153

²²O. Sarig, *Invent. Math.* **150**, 629 (2002). 1154

²³S. Gouëzel, *Isr. J. Math.* **139**, 29 (2004). 1155

²⁴K. K. Lin, *Nonlinearity* **18**, 659 (2005). 1156

²⁵V. Araújo and A. Tahzibi, *Nonlinearity* **18**, 939 (2005). 1157

²⁶M. Blank, *Discrete Contin. Dyn. Syst.* **21**, 749 (2008). 1158

²⁷V. Baladi and M. Viana, *Ann. Sci. Ec. Normale Super.* **29**, 483 (1996). 1159

²⁸M. Jakobson, *Commun. Math. Phys.* **81**, 39 (1981). 1160

²⁹J. Alves and V. Araújo, *Asterisque* **286**, 25 (2003). 1161

³⁰M. Viana, *Brazilian Mathematics Colloquium 1997*, IMPA. 1162

³¹E. W. Hobson, *The Theory of Functions of a Real Variable* (Dover, New York, 1927), Vol. 2. 1163

³²R. Strichartz, *A Guide to Distribution Theory and Fourier Transform* (World Scientific, Singapore, 2003). 1165

AUTHOR QUERIES — 026904CHA

- #1 Author, because of the number of changes to your article, please check your corrections carefully and send us an email with your approval or any minor corrections you may still have. Thank you.